




Transmission spectra of the driven, dissipative Rabi model in the ultrastrong-coupling regimeL. Magazzù ¹, P. Forn-Díaz ^{2,3} and M. Grifoni ¹¹*Institute for Theoretical Physics, University of Regensburg, 93040 Regensburg, Germany*²*Institut de Física d'Altes Energies (IFAE), Barcelona Institute of Science and Technology (BIST), Bellaterra (Barcelona) 08193, Spain*³*Qilimanjaro Quantum Tech SL, Barcelona 08007, Spain*

(Received 9 May 2021; accepted 28 October 2021; published 18 November 2021)

We present theoretical transmission spectra of a strongly driven, damped flux qubit coupled to a dissipative resonator in the ultrastrong-coupling regime. Such a qubit-oscillator system, described within a dissipative Rabi model, constitutes the building block of superconducting circuit QED platforms. The addition of a strong drive allows one to characterize the system properties and study novel phenomena, leading to a better understanding and control of the qubit-oscillator system. In this work, the calculated transmission of a weak probe field quantifies the response of the qubit, in frequency domain, under the influence of the quantized resonator and of the strong microwave drive. We find distinctive features of the entangled driven qubit-resonator spectrum, namely resonant features and avoided crossings, modified by the presence of the dissipative environment. The magnitude, positions, and broadening of these features are determined by the interplay among qubit-oscillator detuning, the strength of their coupling, the driving amplitude, and the interaction with the heat bath. This work establishes the theoretical basis for future experiments in the driven ultrastrong-coupling regime.

DOI: [10.1103/PhysRevA.104.053711](https://doi.org/10.1103/PhysRevA.104.053711)**I. INTRODUCTION**

Current developments in Circuit quantum electrodynamics (QED) are establishing superconducting devices as leading platforms for quantum information and simulations [1–5]. In particular, quantum optics experiments with qubits coupled to superconducting resonators are now performed in (and beyond) the so-called ultrastrong-coupling (USC) regime, with the qubit-resonator coupling reaching the same order of magnitude as the qubit splitting and resonator frequency [6–16]. The strong entanglement between light and matter in the USC regime carries the potential for designing novel quantum hybrid states and for achieving ultrafast information transfer [17].

In circuit QED platforms, the qubits are essentially based on superconducting loops interrupted by Josephson junctions, the nonlinear elements that provide the anharmonicity required to single out the two lowest energy states [18]. In the flux configuration [19], the qubit states are superpositions of clockwise and anticlockwise circulating supercurrents, corresponding to the two lowest energy eigenstates of a double-well potential *seen* by the flux coordinate. The double well can be biased by applying an external magnetic flux, and transitions between states in this qubit basis, where the states are localized in the wells, occur via tunneling through the potential barrier.

The standard theoretical tool to account for the coupling of superconducting qubits to their electromagnetic or phononic environments is provided by the spin-boson model, consisting of a quantum two-level system interacting with a heat bath of harmonic oscillators [20,21]. This model has been the subject of extensive studies as an archetype of dissipation in

quantum mechanics, and the different coupling regimes of spin-boson systems and the associated dynamical behaviors have been theoretically explored by using a variety of approaches [21,22]. Only recently though, progress in the design of superconducting circuits has opened the possibility of attaining experimental control on the strong qubit-environment coupling regime [23–28].

In circuit QED, an appropriate description for qubit-resonator systems is provided by the Rabi Hamiltonian, whose interaction part is featured by terms known as rotating and counterrotating terms. In this context, USC refers to an interaction regime where the rotating wave approximation, which allows for a description in terms of the Jaynes-Cummings Hamiltonian, appropriate for atom-cavity systems, fails, as the counterrotating terms cannot be neglected [15,16]. A refined classification of the different regimes of the Rabi model is provided in [29]. The USC regime of circuit QED is still the subject of much theoretical work; see for example [10,11,30–33]. However, the intricacies of the driven Rabi problem in the USC regime [34] have been largely unexplored so far. Experiments on strongly driven qubits have demonstrated the possibility of controlling properties of engineered quantum two-level systems by intense light [25,35,36]. For example, complex Landau-Zener patterns of avoided crossings could be controlled by tuning the driving amplitude, in agreement with theoretical expectations [5,37–39]. In recent works, spectroscopical signatures of drive-induced new symmetries [40] and nonadiabatic effects [41] in quantum systems have been addressed.

Experimentally, transmission spectroscopy has been shown to be a powerful tool to characterize the complex spectrum of the Rabi problem [9,13,14,42]. Usually, the probe couples to

the resonator, from which properties of the qubit can be inferred. As shown in this work, a probe coupled to the qubit can also provide precious information. Alternatives to the spectroscopy of the qubit to investigate USC systems exist. For example, spectroscopy of ancillary qubits has been proposed in [43] to probe the ground states of ultrastrongly coupled systems. Moreover, methods alternative to the analysis of the transmission spectra have been recently devised to probe the USC regime [44,45].

In this work, we consider a dissipative flux qubit ultrastrongly coupled to a superconducting resonator, modeled as a harmonic oscillator, which in turn interacts with a bosonic heat bath. The qubit is probed by a weak incoming field whose transmitted part provides information on the dynamics under the influence of the resonator and its environment, as demonstrated in a variety of experiments [46–50]. In addition, the qubit is subject to an intense microwave field, the drive. Despite the rich literature on the topic, the impact of an intense microwave drive on the dissipative Rabi model in the USC regime has not been investigated so far. The setup considered describes quantum optics experiments in circuit QED but also the coupling of a qubit to a detector [51–53], and the qubit-bath coupling mediated by a waveguide resonator in a heat transport platform in the quantum regime [54].

We address the spectral properties of the driven USC system in a twofold way. On the one hand, quasienergy spectra of the driven and closed Rabi model are studied analytically using the Floquet–Van Vleck approach of Ref. [34]. On the other hand, the transmission spectra of the open Rabi model are first numerically evaluated in the absence of the pump drive in the weak- and strong-dissipation regimes. This allows us to set up the impact of dissipation on this strongly entangled quantum system. In a last step, the full driven, open USC system is analyzed. We notice that weak dissipation affecting the USC system as a whole can be treated via a master equation approach, e.g., along the lines of [8,55]. Since our USC system is probed through the qubit, we conveniently map the dissipative Rabi model to an effective spin-boson model where the spin interacts directly with a bosonic bath characterized by an effective spectral density. The latter function is peaked at the oscillator frequency [56], and thus describes a so-called structured environment. Using the same approach as the one developed in [25,57] to analyze the measured transmission of a probe field in the presence of an Ohmic environment, here we first calculate the transmission spectra of the undriven qubit, considering different qubit-resonator coupling strengths. Specifically, according to the dissipation regime, the qubit response function is evaluated by using the weak USC system-environment approach developed in [58] or within the so-called noninteracting blip approximation (NIBA), which allows one to treat dissipation (and hence the effects of the resonator) in a nonperturbative way [37]. Finally, we look at the impact of a strong pump field within the NIBA.

The qualitative difference between the setup of Ref. [25], featuring a driven qubit ultrastrongly coupled to an Ohmic environment, and the one in this work, where the driven qubit is ultrastrongly coupled to a dissipative quantum resonator, is reflected in the transmission spectra. In absence of the drive, the spectra show clear signatures of the entanglement between qubit and resonator in the form of avoided crossings and

resonances, whose positions depend on the qubit-resonator coupling strength. Furthermore, renormalization effects due to the dissipative environment have to be properly taken into account for a quantitative description. When the drive is added, novel avoided crossings and resonances reveal the interplay between the resonator photons and the driving field.

The paper is structured as follows. In Sec. II, the driven, dissipative Rabi model and its mapping to an effective, driven spin boson model is discussed. In Sec. III, spectral properties of the nondissipative Rabi model in the USC regime are analyzed, while a formal expression for the transmission is reported in Sec. IV. Numerical results are shown in Sec. V, and interpreted on the basis of the analytical results of Sec. III. Finally, conclusions are drawn in Sec. VI.

II. THE DRIVEN, DISSIPATIVE RABI MODEL

For a realistic description of experiments studying USC systems, the inclusion of decoherence and dissipative effects induced by the electromagnetic environment or by other sources is unavoidable. Previous work used a modified master equation to include the effect of dissipation in the perturbative USC regime [8,55,59]. In the following, we consider a driven, dissipative flux qubit coupled to a resonator which is in turn subject to dissipation. Specifically, qubit and resonator interact with two independent Ohmic heat baths, denoted by 1 and r, respectively. The qubit is characterized by the tunneling matrix element Δ , while the resonator is modeled as a harmonic oscillator of frequency Ω . These two systems are coupled with an interaction strength quantified by the frequency g . If g is of the order of Δ and Ω the system is in the ultrastrong-coupling regime. The full Hamiltonian of this driven, dissipative Rabi model, which is sketched in Fig. 1(a), is

$$\begin{aligned}
 H(t) = & -\frac{\hbar}{2}[\Delta\sigma_x + \epsilon(t)\sigma_z] + \hbar\Omega B^\dagger B - \hbar\sigma_z g(B^\dagger + B) \\
 & + \sum_{k=1}^{N_1} \hbar\omega_{1k} b_{1k}^\dagger b_{1k} - \frac{\hbar}{2}\sigma_z \sum_{k=1}^{N_1} \lambda_{1k} (b_{1k}^\dagger + b_{1k}) \\
 & + \sum_{k=1}^{N_r} \hbar\omega_{rk} b_{rk}^\dagger b_{rk} - \hbar(B^\dagger + B) \sum_{k=1}^{N_r} \lambda_{rk} (b_{rk}^\dagger + b_{rk}) \\
 & + \hbar(B^\dagger + B)^2 \sum_{k=1}^{N_r} \frac{\lambda_{rk}^2}{\omega_{rk}}, \quad (1)
 \end{aligned}$$

see Appendix A, where the qubit operators $\sigma_z = |\downarrow\rangle\langle\downarrow| - |\uparrow\rangle\langle\uparrow|$ and $\sigma_x = |\downarrow\rangle\langle\uparrow| + |\uparrow\rangle\langle\downarrow|$ are expressed in the so-called qubit basis of localized right- and left-well states $|\downarrow\rangle, |\uparrow\rangle$. The qubit is driven by the time-dependent bias

$$\epsilon(t) = \epsilon_0 + \epsilon_p \cos(\omega_p t) + \epsilon_d \cos(\omega_d t), \quad (2)$$

which is the sum of a static part ϵ_0 , a weak probe (p), and a drive (d) with arbitrary amplitude, which we will assume to be of high frequency; see Fig. 1(c).

The bosonic creation and annihilation operators $B^\dagger, b_{1/rk}^\dagger$ and $B, b_{1/rk}$ create and destroy an excitation in the resonator and in the k th harmonic oscillator of the qubit/resonator bath, respectively. The angular frequencies $\lambda_{1/rk}$ correspond to the coupling strengths with the individual modes of the

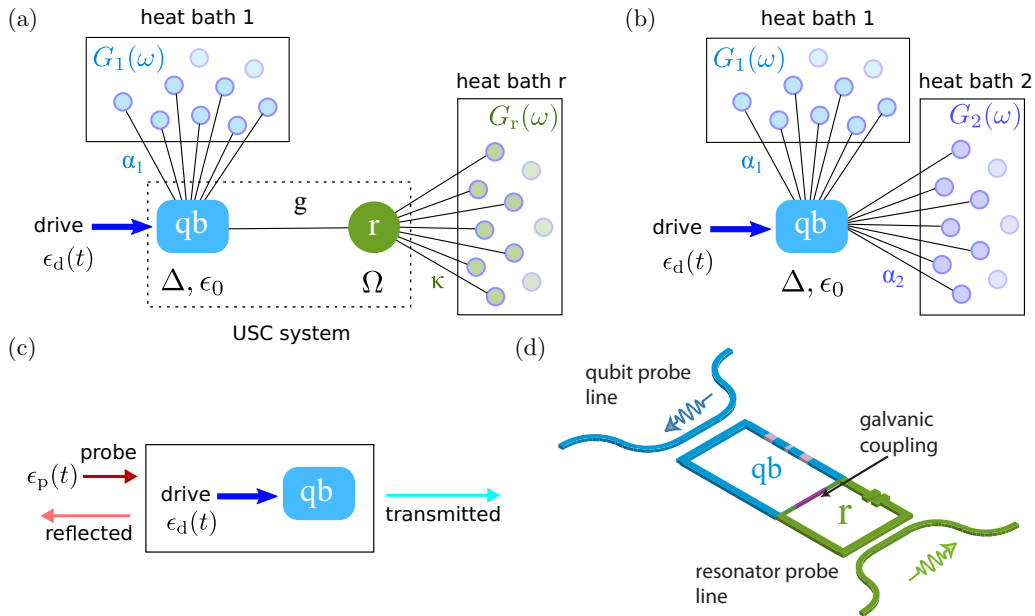


FIG. 1. Model and experimental design of the driven dissipative Rabi model. (a) The dissipative Rabi model is realized by coupling a flux qubit to an Ohmic heat bath, denoted with 1, and to a resonator, which is in turn coupled to an Ohmic environment, denoted with r . (b) The model is mapped into a two-bath spin-boson model, where the qubit is coupled to two heat baths. The first is the original bath 1 while the second, denoted by 2, is a structured effective bath. (c) Detail of the two-tone spectroscopy protocol where the transmission line is used to probe the driven qubit, the drive being applied via the transmission line as well. (d) Simplified circuit implementation of the USC system displaying the qubit (large loop interrupted by three Josephson junctions) and the LC resonator (smaller loop). The qubit and resonator are galvanically connected to enhance the coupling strength into the USC regime. The qubit and resonator probing lines correspond to their respective Ohmic environments.

respective baths. Note that by removing the resonator and its bath from the full Hamiltonian (1), we are left with the standard spin-boson Hamiltonian [20]. On the other hand, removing the baths coupled to qubit and resonator, the standard Rabi Hamiltonian is recovered.

Each bath is fully characterized by the spectral density function

$$G(\omega) = \sum_k \lambda_k^2 \delta(\omega - \omega_k). \quad (3)$$

In the continuum limit, we assume an Ohmic spectral density with exponential cutoff for the qubit, i.e., $G_1(\omega) = 2\alpha_1\omega e^{-\omega/\omega_c}$, with ω_c a high-frequency cutoff, and a strictly Ohmic spectral density $G_r(\omega) = \kappa\omega$ for the resonator. The dimensionless dissipation strengths are related to the friction coefficient in the Caldeira-Leggett model [21,60,61]; see Appendix A.

Figure 1(d) shows a schematic of the implementation of the driven, dissipative Rabi model using a superconducting circuit. A 3-junction flux qubit is galvanically attached to an LC resonator in order to attain ultrastrong-coupling strengths, while keeping the interaction linear. In addition, two superconducting waveguides couple to the qubit and resonator, in order to define their own respective Ohmic baths. The coupling to the baths determines the decay rate of each system, with an additional loss channel due to intrinsic microscopic noise present in the neighborhood of the circuit. In order to experimentally implement the system proposed in this work, coupling strengths in the range $g/\Omega = 0.3-0.5$ are most suitable. Coupling strengths $g/\Omega > 1$ have already been achieved

in qubit-resonator systems employing shared Josephson junctions as couplers [13]. While providing the desired coupling strength, the junctions also contain a nonlinearity that may introduce modifications to the standard Rabi model. Using linear inductors it is also possible to attain ultrastrong couplings [12]. Thin-film aluminum would require a shared wire of significant length due to its low kinetic inductance. An alternative is to employ superinductance material compatible with aluminum such as granular aluminum [62,63]. This material behaves as a linear inductor up to very large currents with inductances 0.1–1 nH per unit area and is therefore very suitable as an ultrastrong qubit-resonator coupler. In our coupling regimes of interest, we can estimate the necessary parameters using $g/\Omega = L_c I_p \{ [2\Omega(L_c + L_r)]/\hbar \}^{-1/2}$, which yields the desired range 0.3–0.5, with qubit persistent current $I_p = 100$ nA, shared coupling inductance $L_c = 0.4$ nH, resonator inductance $L_r = 3.5$ nH, and resonator frequency $\Omega/2\pi = 1$ GHz.

The full Hamiltonian of the model, Eq. (1), can be mapped to that of the two-bath spin-boson model depicted in Fig. 1(b), which reads

$$H_{SB}(t) = -\frac{\hbar}{2}[\Delta\sigma_x + \epsilon(t)\sigma_z] - \frac{\hbar}{2}\sigma_z \sum_{vk} \lambda_{vk}(a_{vk}^\dagger + a_{vk}) + \sum_{vk} \hbar\omega_{vk} a_{vk}^\dagger a_{vk}. \quad (4)$$

In this effective Hamiltonian, the qubit is directly coupled to two bosonic baths indexed with $\nu = 1, 2$: the bath 1 is the same Ohmic bath coupled to the qubit as in Eq. (1). The

second, $\nu = 2$, is a new, *effective* bath whose spectral density, in the continuum limit, reads [52,56,64–66]

$$G_2(\omega) = \frac{2\alpha_2\omega\Omega^4}{(\Omega^2 - \omega^2)^2 + (\gamma\omega)^2}. \quad (5)$$

This effective spectral density is structured, meaning that it displays a peak centered at the oscillator frequency Ω with width $\gamma = 2\pi\kappa\Omega$. The latter frequency is the memoryless damping kernel of the resonator's Ohmic bath; see Appendix A. The corresponding effective coupling strength α_2 is given by the dimensionless parameter $\alpha_2 = 8\kappa g^2/\Omega^2$. In the limit $\Omega \gg \Delta$ the qubit sees a bath with a low-frequency Ohmic behavior. By taking the limit $\kappa \rightarrow 0$ (i.e., disconnecting the Ohmic bath interacting with the resonator), we obtain $\lim_{\kappa \rightarrow 0} G_2(\omega) = 4g^2\delta(\omega - \Omega)$, which consistently describes the bath $\nu = 2$ as comprising a single oscillator coupled to the qubit with strength $\lambda = 2g$. The resulting interaction term in Eq. (4) reproduces the qubit-resonator coupling term in Eq. (1). This problem displays high complexity due to the strong driving on the qubit, the ultrastrong coupling between qubit and resonator, as well as environmental effects on both qubit and oscillator. In order to gain physical insight, we first recall some features of the spectrum of the driven Rabi system in the absence of dissipation.

III. ANALYTICAL TREATMENT OF THE CLOSED RABI MODEL IN THE USC REGIME

A. Closed Rabi model in the USC regime

We start with the nondriven, nondissipative Rabi model, whose spectrum has been discussed in various works by now; see, e.g., [8,10,11,67,68]. Because of the coupling to the qubit, the states of the resonator are displaced in one of two opposite directions depending on the persistent-current state of the qubit. In mathematical terms, this gives rise to displaced coherent states of the oscillator. The energy eigenstates of the Rabi system are then a coherent superposition of product states for the qubit and the displaced oscillator. Following the polaron approach, an approximate analytical expression for the spectrum of the Rabi model can be derived using Van Vleck perturbation theory in the qubit's tunneling parameter Δ . The approximation is nonperturbative in the qubit-resonator coupling strength g and performs excellently [11] for negative detuning ($\Omega > \Delta$).

For $\Delta = 0$, the eigenstates of the system are composed of tensor products of displaced oscillator and qubit eigenstates. The exact spectrum is given by the combination of qubit and resonator energies

$$E_{\mp,j} = \mp \frac{\hbar}{2}\epsilon_0 + \hbar j\Omega - \hbar \frac{g^2}{\Omega}, \quad j = 0, 1, 2, \dots \quad (6)$$

A finite tunneling Δ mixes the eigenstates nontrivially. To find an approximate analytical solution, we notice that for static bias values $\epsilon_0 = l\Omega$ one can identify twofold-degenerate subspaces in the complete Hilbert space of the problem: $E_{+,j} = E_{-,l}$. A finite tunneling removes the degeneracy and induces coupling among the dressed states. Using Van Vleck perturbation theory to lowest order in the tunneling one finds

the modified energies [11]

$$E_{\mp,j}^l \simeq \hbar \left[\left(j + \frac{l}{2} \right) \Omega - \frac{g^2}{\Omega} + \frac{1}{8} (\varepsilon_{\downarrow,j}^{(2),l} - \varepsilon_{\uparrow,j+l}^{(2),l}) \mp \frac{1}{2} \Omega_j^l \right], \quad (7)$$

where l identifies the degeneracy points $\epsilon_0 = l\Omega$. For example, around $\epsilon_0 = 0$ the energy levels are, in ascending order, $E_{-,0}^0, E_{+,0}^0, E_{-,1}^0, \dots$, and around $\epsilon_0 = \Omega$ they are given by $E_{-,0}^1, E_{+,0}^1, E_{-,1}^1, \dots$, while for $\epsilon_0 = -\Omega$ we have $E_{-,0}^{-1}, E_{-,1}^{-1}, E_{+,1}^{-1}, \dots$. For the level splitting in Eq. (7) it is found

$$\Omega_j^l = \sqrt{\left[\epsilon_0 - l\Omega + \frac{1}{4} (\varepsilon_{\downarrow,j}^{(2),l} + \varepsilon_{\uparrow,j+l}^{(2),l}) \right]^2 + (\Delta_j^{j+l})^2}, \quad (8)$$

where the so-called diagonal corrections are given by

$$\varepsilon_{\downarrow/\uparrow,j}^{(2),l} = \sum_{\substack{k=-j \\ k \neq \pm l}}^{\infty} \frac{(\Delta_j^{k+j})^2}{\epsilon_0 \mp k\Omega}. \quad (9)$$

The dressed tunneling elements carry information on the overlap of the displaced oscillator states. They read

$$\Delta_j^{j'} = \Delta [\text{sgn}(j' - j)]^{|j'-j|} D_{\min\{j,j'\}}^{|j'-j|}(\tilde{\alpha}), \quad (10)$$

with j and j' the number of oscillator quanta involved in the dressing,

$$D_j^k(\tilde{\alpha}) = \tilde{\alpha}^{k/2} \sqrt{\frac{j!}{(j+k)!}} \mathbb{L}_j^k(\tilde{\alpha}) e^{-\frac{\tilde{\alpha}}{2}}, \quad (11)$$

and $\tilde{\alpha} = (2g/\Omega)^2$. Here, $\mathbb{L}_j^k(\tilde{\alpha})$ are the generalized Laguerre polynomials defined by the recurrence relation

$$\mathbb{L}_{j+1}^k(\tilde{\alpha}) = \frac{(2j+1+k-\tilde{\alpha})\mathbb{L}_j^k(\tilde{\alpha}) - (j+k)\mathbb{L}_{j-1}^k(\tilde{\alpha})}{j+1}, \quad (12)$$

with $\mathbb{L}_0^k(\tilde{\alpha}) = 1$ and $\mathbb{L}_1^k(\tilde{\alpha}) = 1+k-\tilde{\alpha}$. For $|\epsilon_0| < \Omega$ we fix $l = 0$.

For $\Omega = \epsilon_0$, corresponding to $l = 1$, one finds for the avoided crossing involving the first and second excited state, $\Delta_0^1 = \Delta\sqrt{\tilde{\alpha}}e^{-\tilde{\alpha}/2}$. In the limit of small $\tilde{\alpha}$, one can expand the dressed tunneling splittings in order to obtain the famous Rabi splitting of the Jaynes-Cummings model which, at resonance, assumes the value $2\hbar g\sqrt{j+1}$. Noticeably, in the high-photon limit, $j, j' \rightarrow \infty$, and for finite $j-j'$, this dressing by Laguerre polynomials becomes a dressing by Bessel functions known for quantum systems under intense electromagnetic fields [37]. The interplay between quantum and classical radiation is the topic of the next subsection.

B. Driven Rabi model

We include now a drive on the qubit. The picture is enriched, with respect to the static case, by the presence of new resonances and by the modulation induced by the Bessel functions, which stems from the classical drive, on top of the Laguerre dressing given by the quantum oscillator, i.e., the resonator. The spectrum can now be calculated within a

dressed Floquet picture, with quasienergies known exactly for the case $\Delta = 0$. Similarly to the static case, twofold degeneracies now occur when $\epsilon_0 = l\Omega - m\omega_d$. Within leading order

Floquet–Van Vleck perturbation theory in Δ , the quasienergy spectrum of the driven, nondissipative Rabi model now reads¹ [34]

$$E_{\mp, n, j}^{m, l} = \hbar \left[-\left(n + \frac{m}{2}\right)\omega_d + \left(j + \frac{l}{2}\right)\Omega - \frac{g^2}{\Omega} + \frac{1}{8}(\epsilon_{\downarrow, n, j}^{(2), m, l} - \epsilon_{\uparrow, n+m, j+1}^{(2), m, l}) \mp \frac{1}{2}\Omega_{n, j}^{m, l} \right], \quad (13)$$

where the indexes n and j denote the Floquet mode and oscillator quantum number, respectively, while m and l give the resonance condition. The doublets' amplitudes are now given by, cf. Eq. (8),

$$\Omega_{n, j}^{m, l} \simeq \sqrt{\left[\epsilon_0 + m\omega_d - l\Omega + \frac{1}{4}(\epsilon_{\downarrow, n, j}^{(2), m, l} + \epsilon_{\uparrow, n+m, j+1}^{(2), m, l}) \right]^2 + (\Delta_{n, j}^{n+m, j+|l|})^2}, \quad (14)$$

where the diagonal corrections read

$$\epsilon_{\downarrow/\uparrow, n, j}^{(2), m, l} = \sum_{\substack{p=-\infty \\ p \neq -m}}^{\infty} \sum_{\substack{k=-j \\ k \neq \pm l}}^{\infty} \frac{(\Delta_{n, j}^{n+p, j+k})^2}{\epsilon_0 + p\omega_d \mp k\Omega}. \quad (15)$$

The tunneling elements are further dressed by Bessel functions as

$$\Delta_{n, j}^{n', j'} = J_{n'-n}(\epsilon_d/\omega_d)\Delta_j^{j'}, \quad (16)$$

with $\Delta_j^{j'}$ defined in Eq. (10). Noticeably, the bare tunneling splitting is now dressed by *both* quanta of the resonator and of the driving microwave radiation.

At the symmetry point, $\epsilon_0 = 0$, the resonances still occur when $m\omega_d \simeq l\Omega$. For example, in the case $m = 1$, $l = 2$, one finds avoided crossings with tunneling splitting $\Delta_{n, j}^{n+1, j+2} = J_1(\epsilon_d/\omega_d)\Delta_j^{j+2}$. As we shall see in Sec. V, these resonances dominate the low-energy transmission of the driven Rabi model for the chosen parameter set. Before this, we illustrate in the coming section how to relate the qubit transmission spectra, namely the spectral properties of the Rabi model as probed in the experimental setup, see Figs. 1(c) and 1(d), to the steady-state response of the qubit.

IV. TRANSMISSION

In actual experiments, see Fig. 1(c), the probe field $V_{\text{in}}^{\text{p}}(t) = f_Z \epsilon_p \cos(\omega_p t)$ is applied to the qubit via an external transmission line. Following [25, 69], the corresponding transmitted field is $V_{\text{transm}}(t) = V_{\text{in}}^{\text{p}}(t) - f\dot{P}(t)/2$, where $P(t) := \langle \sigma_z(t) \rangle$ is the so-called qubit population difference in the localized qubit basis. The proportionality constants f_Z and f depend on the details of the experimental setup and have dimensions of a magnetic flux. In terms of the Fourier-transformed probe and transmitted fields calculated at the probe frequency, the transmission is defined as the square modulus of the complex coefficient

$$\mathcal{T}(\omega_p) = \tilde{V}_{\text{transm}}(\omega_p)/\tilde{V}_{\text{in}}^{\text{p}}(\omega_p). \quad (17)$$

At the steady state, the population difference has the period of the probe, also in the presence of a high-frequency drive,

provided that we average over its period $2\pi/\omega_d$ the kernels of the exact generalized master equation (GME) for $P(t)$; see Appendix B. Expanding in Fourier series the time-periodic asymptotic population difference $P_{\text{as}}(t) = \lim_{t \rightarrow \infty} P(t)$ as²

$$\dot{P}_{\text{as}}(t) = \sum_m -im\omega_p p_m e^{-im\omega_p t}, \quad (18)$$

where

$$p_m = \frac{\omega_p}{2\pi} \int_{-\pi/\omega_p}^{\pi/\omega_p} dt P_{\text{as}}(t) e^{im\omega_p t}, \quad (19)$$

we find for the transmission at the probe frequency ω_p , within linear response to the probe field,

$$\mathcal{T}(\omega_p) = 1 + i\mathcal{N}\hbar\omega_p\chi(\omega_p), \quad (20)$$

where $\mathcal{N} = f/f_Z$ and $\chi(\omega_p) = p_1/\hbar\epsilon_p$. Hence, the theoretical quantity of interest is the linear susceptibility evaluated at the probe frequency. Its form depends on the considered dissipation regime. In the next subsection we provide an explicit approximate expression for the response function.

Linear susceptibility within the NIBA

Within the NIBA [20, 21, 70], the GME that describes the driven, dissipative qubit dynamics yields an analytical expression for the linear susceptibility $\chi(\omega_p)$, see Appendix C, which is nonperturbative in the qubit-baths coupling. It reads

$$\chi(\omega_p) = \frac{(\hbar\omega_p)^{-1}}{-i\omega_p + \hat{k}_0^{\pm}(-i\omega_p)} \left[\hat{k}_{+1}^{-}(0) - \hat{k}_{+1}^{+}(0) \frac{\hat{k}_0^{-}(0)}{\hat{k}_0^{+}(0)} \right], \quad (21)$$

where the GME kernels are defined as

$$\begin{aligned} \hat{k}_0^{\pm}(\lambda) &= \Delta^2 \int_0^{\infty} d\tau e^{-\lambda\tau} e^{-Q'(\tau)} c^{\pm}[Q''(\tau)] \\ &\quad \times J_0 \left[\frac{2\epsilon_d}{\omega_d} \sin\left(\frac{\omega_d\tau}{2}\right) \right] c^{\pm}(\epsilon_0\tau), \\ \hat{k}_1^{\pm}(0) &= \mp \Delta^2 \int_0^{\infty} d\tau e^{i\omega_p\tau/2} e^{-Q'(\tau)} c^{\pm}[Q''(\tau)] \\ &\quad \times J_0 \left[\frac{2\epsilon_d}{\omega_d} \sin\left(\frac{\omega_d\tau}{2}\right) \right] \sin(\omega_p\tau/2) c^{\mp}(\epsilon_0\tau), \end{aligned} \quad (22)$$

¹We keep the same convention for the indexes as in [11].

²Note the different convention used for the signs with respect to Ref. [25].

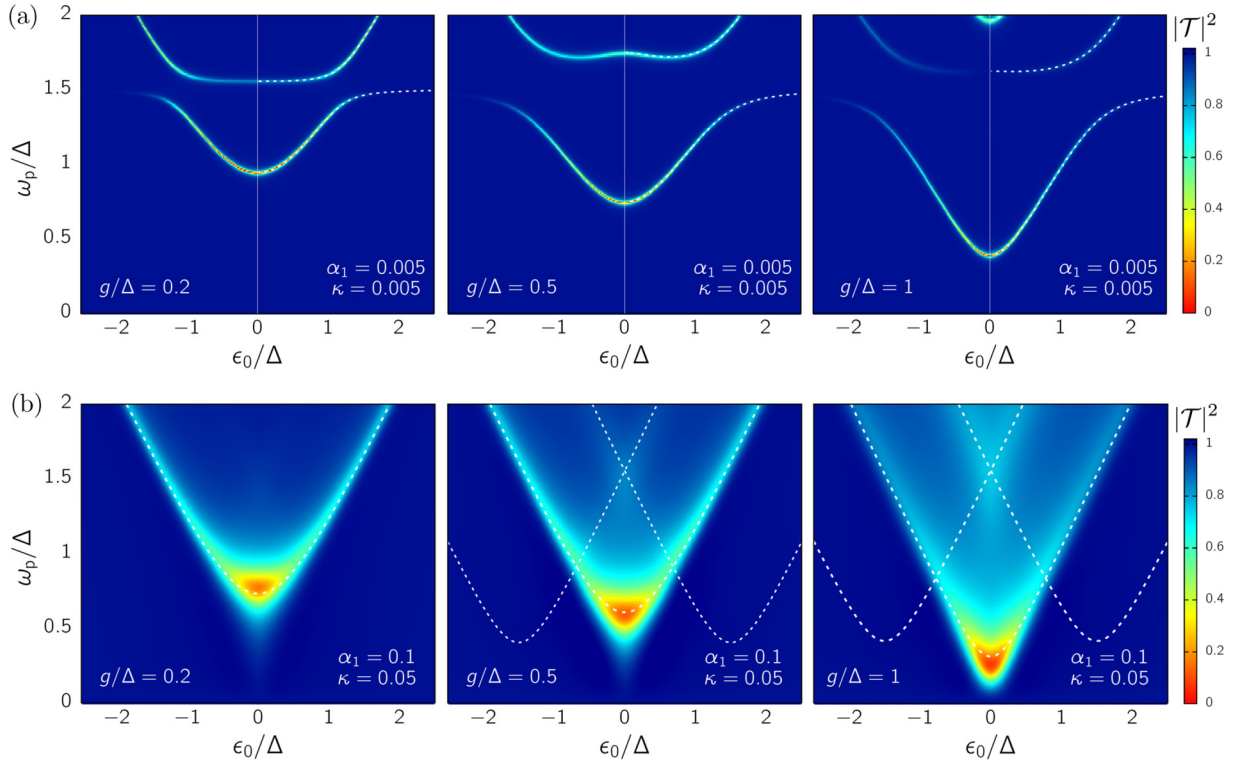


FIG. 2. Transmission spectra of the static system with resonator frequency $\Omega = 1.5\Delta$ and different values of the qubit-resonator coupling g . The transmission is evaluated using Eq. (20) with \mathcal{N} chosen differently for each plot in order to have the minimum of the transmission assuming the value $|\mathcal{T}|^2 \simeq 0$. (a) Weak dissipation: The susceptibility $\chi(\omega_p)$ is calculated using the approach of [58] with dephasing rates from the Bloch-Redfield master equation in the *dressed* basis of the USC system. The dashed white lines are the transition energies between the ground and the first excited states of the closed Rabi model obtained by numerical diagonalization. The resonator's Hilbert space is truncated to the first 10 energy levels. (b) Strong dissipation: The susceptibility is calculated with the path-integral approach within the NIBA, Eq. (21), starting from the effective bath mapping in Eq. (4). The dashed lines are given by the frequency gaps $\tilde{\Omega}_0^l$, Eq. (24), with $l = 0, \pm 1$. In both panels the cutoff frequency of the qubit bath is $\omega_c = 10\Delta$ and temperature is $k_B T = 0.1\hbar\Delta$ for both baths.

with $c^+(x) = \cos(x)$ and $c^-(x) = \sin(x)$; see also [25,37,57]. Here, $J_0(x)$ is the Bessel function of the first kind [71], which stems from averaging the kernels over the drive period; see Appendix D. The baths' correlation function is the sum $Q(t) = \sum_\nu Q_\nu(t)$, where

$$Q_\nu(t) = \sum_\nu \int_0^\infty d\omega \frac{G_\nu(\omega)}{\omega^2} \times \left[\coth\left(\frac{\hbar\omega\beta_\nu}{2}\right)(1 - \cos\omega t) + i \sin\omega t \right], \quad (23)$$

with $\beta_\nu := (k_B T_\nu)^{-1}$ the inverse temperature of bath ν . Explicit expressions for $Q_\nu(t)$ are provided in Appendix B.

The NIBA is perturbative in the qubit splitting Δ and provides accurate results in the case of zero bias, $\epsilon_0 = 0$, and in the presence of a finite bias for sufficiently strong dissipative coupling and/or high temperatures. This is due to the enhanced downward renormalization of Δ by increasing α and to the fact that the real parts of the correlation functions $Q(t)$ suppress effectively the time-nonlocal correlations in the two-state path integral, rendering the present NIBA treatment appropriate [21]. These considerations hold for both the Ohmic and the effective structured bath acting on the qubit; see Eqs. (B5)–(B10). In the presence of a high-

frequency drive, the additional drive-induced renormalization of the qubit parameter Δ , Eq. (16), extends the reach of this approximation scheme to regimes of lower dissipation. The NIBA has been applied in the presence of multiple baths, notably in the context of heat transport; see, e.g., [72–75].

In the following, for the case of a biased qubit and weak dissipation or low temperatures, we use a weak damping master equation approach. The NIBA is used for strong dissipation and in the presence of a drive in its range of applicability, which includes the unbiased case at weak dissipation. Transmission spectra of the static and driven setup are shown in the following section for both dissipation regimes.

V. TRANSMISSION SPECTRA

In the following, we show the results for the transmission with the probe on the qubit, Eq. (20), with the resonator frequency set to $\Omega = 1.5\Delta$, both in the static case and in the presence of the drive on the qubit. In the latter setting, we fix the drive frequency to the value $\omega_d = 2.7\Delta$. In order to see how the picture of the static Rabi model is impacted by a classical drive on the qubit, we start by showing in Fig. 2 the static case in two dissipation regimes, which in turn provides insight on the effect of dissipation on the spectra.

In the first, where the USC system is weakly coupled to the environment, we calculate the susceptibility $\chi(\omega_p)$ using the approach developed in [58] with dephasing rates from the Bloch-Redfield master equation calculated in the dressed basis of the USC system. In the other regime considered, which is of strong dissipation, we use the path-integral approach within the NIBA, Eqs. (21)–(23), for the spin-boson model with the effective bath mapping, Eq. (4). For both cases, we consider three values of the qubit-resonator coupling, namely $g/\Delta = 0.2, 0.5$, and 1 , the latter two being well into the USC regime. The picture that emerges from the spectra differs, especially at strong dissipation, from the standard spectroscopy of USC systems, where the transmission of a weakly dissipative USC system is recorded by probing the resonator [13]; see Appendix E for a comparison. In our transmission measurement protocol, which essentially measures the qubit operator σ_z , the transmission is given by the difference in populations of the states $|\uparrow\rangle, |\downarrow\rangle$ of the qubit basis. As such, the resonator is traced out from the dynamical response of the system, its presence being reflected in the pattern of resonances involving qubit and resonator. Qualitatively, this leads to a spectrum resembling the one of the qubit alone, with a principal feature, a pronounced dip centered at $\epsilon_0 = 0$, which is faithfully reproduced by the transition frequency $\tilde{\Omega}_0^0$ that is renormalized by the Ohmic bath acting on the qubit. There are, however, two major modifications that are peculiar to the Rabi model. (i) Emission and absorption of l oscillator quanta produce *sidebands* of the main spectral features. (ii) Avoided crossings are visible at weak dissipation, where the environment-induced renormalization of the bare qubit splitting Δ and oscillator frequency Ω are negligible, which signals the strong resonator-qubit entanglement, according to Eqs. (7) and (8).

For our analysis, we introduce the *bath-renormalized* transition frequencies

$$\tilde{\Omega}_j^l = (\tilde{E}_{+,j}^l - \tilde{E}_{-,j}^l)/\hbar, \quad (24)$$

see Eqs. (7) and (8), where $\tilde{E}_{\pm,j}^l$ give the eigenenergies [or quasienergies, with appropriate additional indexes, Eq. (13)] of the closed Rabi model around the bias point $\epsilon_0 = l\Omega$. When comparing with the NIBA results, these renormalized energies are calculated by substituting the bare qubit splitting Δ with its dissipation-renormalized version: $\Delta \rightarrow \Delta_T$, where $\Delta_T = \Delta_r(2\pi k_B T/\hbar \Delta_r)^{\alpha_1}$ and $\Delta_r = \Delta(\Delta/\omega_c)^{[\alpha_1/(1-\alpha_1)]}$ [21].

In the absence of the resonator, the principal dip at zero static bias would occur at $\omega_p \sim \Delta$ for weak dissipation, with a downward renormalization for increased system-bath coupling; see Fig. 2 of Ref. [25]. In Fig. 2, the presence of the (dissipative) resonator moves this principal feature toward lower frequencies upon increasing g . This effect can be understood in terms of the renormalization of Δ by Laguerre polynomials discussed in Sec. III A, see Eq. (10), which yields the spectrum of the Rabi model. Thus, now the main dip is centered at $\omega_p = \tilde{\Omega}_0^0|_{\epsilon_0=0} \simeq \Delta_T \exp(-\tilde{\alpha}/2)$, where $\tilde{\alpha} = (2g/\Omega)^2$. Here and in what follows, we neglect for simplicity the second-order corrections $\varepsilon_{\downarrow/\uparrow,j}^{(2,l)}$, Eq. (9).

The avoided crossings present at weak dissipation, Fig. 2(a), are given by the difference between the transition energies $E_2 - E_0$ and $E_1 - E_0$ at $\epsilon_0 = \Omega$, namely by the

dressed tunneling element $E_2 - E_1 = E_{+,0}^1 - E_{-,0}^1 \simeq |\Delta_0^1| = \Delta \tilde{\alpha}^{1/2} \exp(-\tilde{\alpha}/2)/\sqrt{2}$, see Eqs. (7) and (10), showing a non-monotonic behavior with respect to g . This nonmonotonicity is more evident at resonance (see Fig. 6). The crossing pattern at strong dissipation, Fig. 2(b), in the region $\epsilon_0 \sim 0$ is well reproduced by the frequency gaps $\tilde{\Omega}_0^0$ and $\tilde{\Omega}_0^{\pm 1}$ which render the transitions $|\uparrow\rangle \leftrightarrow |\downarrow\rangle$ with the oscillator in a fixed state l , adiabatically following the qubit transitions [10], which is consistent with a strongly suppressed qubit splitting. We note that the avoided crossings are suppressed by dissipation. Figure 2 shows that, in the static case, there is no response from the qubit outside the region $|\epsilon_0| \leq \omega_p$. This is because, contrary to the driven case, see Fig. 3, the weak probe does not induce qubit transitions as its frequency cannot match the qubit frequency gap $\sqrt{\Delta_T^2 + \epsilon_0^2}$. In Appendix F, we compare, in an intermediate-dissipation regime, the results from the two different approaches used here. Both treatments well reproduce the main resonance involving the ground/first excited state transition. However, in agreement with the findings in Fig. 2, strong differences appear for the higher-lying excitations.

A similar, though richer, picture is revealed by Fig. 3, where we consider the spectra in the same strongly dissipative setting of Fig. 2(b) in the presence of the drive, for three values of the drive amplitude ϵ_d , the first being $\epsilon_d = 0$ for reference. While varying ϵ_d , we fix the coupling to $g = 0.5\Delta$. Here, additional renormalization of Δ with appropriate Bessel functions is expected; see Eqs. (14) and (16). For the main transmission dip, the zero-order Bessel function is involved, and its location is found to be at

$$\omega_p = \tilde{\Omega}_{0,0}^{0,0}|_{\epsilon_0=0} \simeq |\Delta_T \exp(-\tilde{\alpha}/2) J_0(\epsilon_d/\omega_d)|. \quad (25)$$

In the resulting set of spectra, the drive amplitude ϵ_d takes the role played by g in the static case, in that ϵ_d tunes the frequency of the main transmission dip and the size of the drive-induced avoided crossings. A detailed account of this effect for zero static bias is provided in Fig. 4(b). Additional features emerge in the driven case displayed in Fig. 3 which are due to multiple resonances of the bias with the drive frequency. These resonances yield replicas of the Rabi pattern, in the form of sidebands, reproduced by the transition frequencies $\tilde{\Omega}_{0,0}^{0,0}, \tilde{\Omega}_{0,0}^{0,\pm 1}, \tilde{\Omega}_{0,0}^{\pm 1,0}, \tilde{\Omega}_{0,0}^{1,1}$, and $\tilde{\Omega}_{0,0}^{-1,-1}$, the last three involving the drive frequency ω_d ; see Eqs. (13) and (14). An interesting feature emerging by comparison of the central and the right panels of Fig. 3 is that, while the central pattern fades for increased drive amplitude, the side replicas are enhanced, as the strong drive is able to induce these multiphoton transitions (which are absent in the probe-only spectra). Mathematically, this is due to the fact that, depending on the bias, the dressed tunneling element is modulated by Bessel functions $J_n(x)$ with different index n . In the case of Fig. 3, the central pattern, $\epsilon_0 \sim 0$, is modulated by $J_0(\epsilon_d/\omega_d)$ and the side replicas by $J_1(\epsilon_d/\omega_d)$.

Such Bessel pattern is highlighted in Fig. 4. In panel (a), the qubit transmission in the driven case is shown as a function of the static bias and of the drive amplitude, displaying the V-shaped trace centered at zero bias. The modulation by $J_0(\epsilon_d/\omega_d)$ causes the suppression of the qubit response at zero bias when the first zero of J_0 is reached. The plot shows the system's response at a specific probe frequency ω_p . By setting

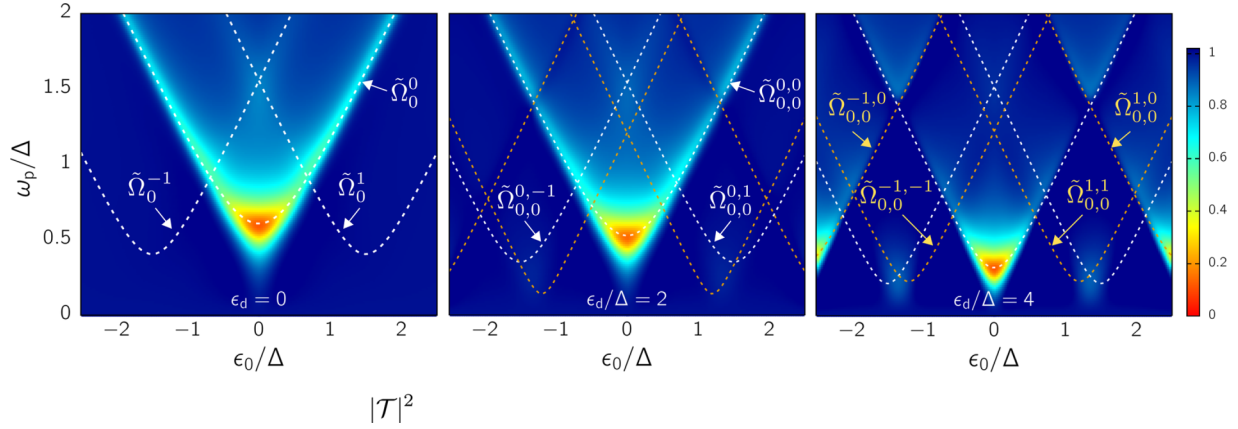


FIG. 3. Transmission spectra of the driven system at strong dissipation. The qubit-resonator coupling is fixed to $g = 0.5\Delta$ and three values of the drive amplitude are considered. From left to right: $\epsilon_d/\Delta = 0, 2$, and 4 . The remaining parameters are as in Fig. 2(b). Note that the panel on the left (static case) coincides with the central panel of Fig. 2(b) with the frequency gaps $\tilde{\Omega}_0^l$ given by Eq. (24). The drive frequency is fixed to the value $\omega_d/\Delta = 2.7$. We note that increasing the driving strength has the twofold effect of downward-renormalizing the frequency of the principal dip a zero bias, similarly to what happens as g is increased in the static system [see Fig. 2(b)], and of creating a pattern of multiphoton resonances described by $\tilde{\Omega}_{0,0}^{m,l}$ [dashed lines, Eqs. (14) and (24)]. The golden dashed lines, $m \neq 0$, involve the drive frequency ω_d .

the static bias to zero, we study in Fig. 4(b) the full spectrum vs the drive amplitude at weak dissipation, a regime where the NIBA is reliable for $\epsilon_0 = 0$ [65]. Such spectrum reveals that the renormalized transition frequency $\tilde{\Omega}_0^0$ follows the Bessel pattern induced by $J_0(\epsilon_d/\omega_d)$ as suggested by Eq. (16).

The same is true for both panels of Fig. 5, where we show the spectrum at zero static bias as a function of the qubit-resonator coupling strength, for $\epsilon_d = 0$ and $\epsilon_d = 4\Delta$. In panel (a), the features in the transmission are reproduced by the transition frequencies in Eq. (8) with $\Delta \rightarrow \Delta_T$. Panel (b) of Fig. 5 shows that the condition $l = 0$ at zero bias, used for the spectrum of the static system, is no more generally true. Indeed, as can be seen from Eq. (14), the drive introduces novel resonance conditions with $l \neq 0$, i.e., when $l\Omega \simeq m\omega_d$. In turn, this allows the contribution of dressed tunneling

elements of the type $\Delta_{n,j}^{n+m,j+l}$. By inspection of Eqs. (10) and (13)–(16), we see that, if $m = 1$ and $l = 2$, the dressing involves $J_1(\epsilon_d/\omega_d)\tilde{\alpha}L_j^2(\tilde{\alpha})\exp(-\tilde{\alpha}/2)$, which, already for $j = 0$, yields a nonmonotonic behavior of the corresponding resonance with respect to $\tilde{\alpha} = (2g/\Omega)^2$. The combined effect of the different resonances in the presence of the driving at $\epsilon_0 = 0$ is the splitting of the main resonance in Fig. 5(b). This feature is not visible in the absence of driving, Fig. 5(a), because $l = 0$ and the resulting dressed tunneling element Δ_j^j in Eq. (8) yields a simple exponential suppression.

VI. CONCLUSIONS

We have theoretically investigated the transmission spectra of the driven, dissipative Rabi model in the USC regime.

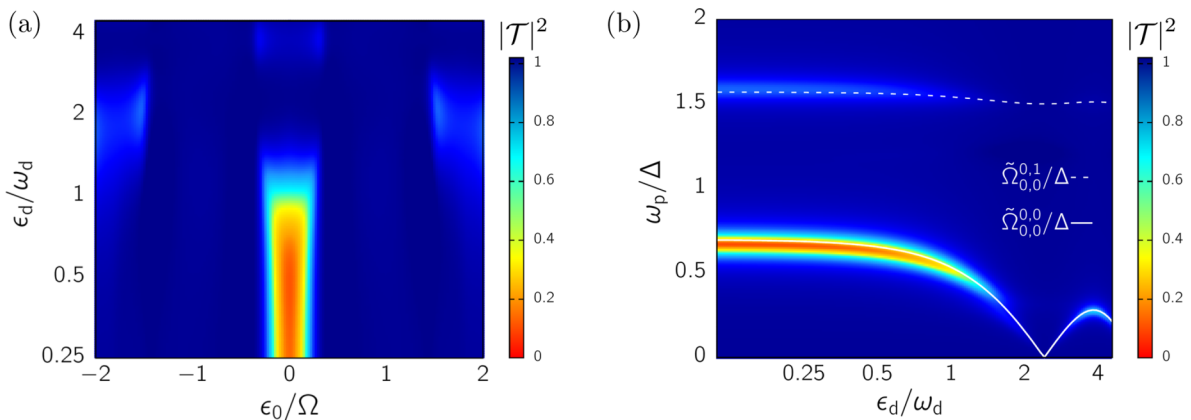


FIG. 4. Bessel pattern from drive-induced renormalization of the resonances. (a) Transmission as a function of the static bias ϵ_0 and of the drive amplitude ϵ_d , at fixed probe frequency $\omega_p/\Delta = 0.55$ and with $\alpha_1 = 0.1$ and $\kappa = 0.05$. (b) Transmission spectrum, as a function of the drive amplitude, for $\epsilon_0 = 0$, at lower dissipation strength, $\alpha_1 = 0.05$ and $\kappa = 0.005$. For both panels, the remaining parameters are as in Fig. 3. The solid and dashed curves in panel (b) are given by the renormalized transition frequencies $\tilde{\Omega}_{0,0}^{0,l}$, see Eqs. (14) and (24), where in the present unbiased case, $\tilde{\Omega}_{0,0}^{0,+1} = \tilde{\Omega}_{0,0}^{0,-1}$. In the transition frequency $\tilde{\Omega}_{0,0}^{0,0}$ it is clearly visible the Bessel pattern induced by the function $J_0(\epsilon_d/\omega_d)$ due to the drive; see Eq. (25). In particular, the dip at $\epsilon_d/\omega_d \approx 2.4$ corresponds to the first zero of such Bessel function.

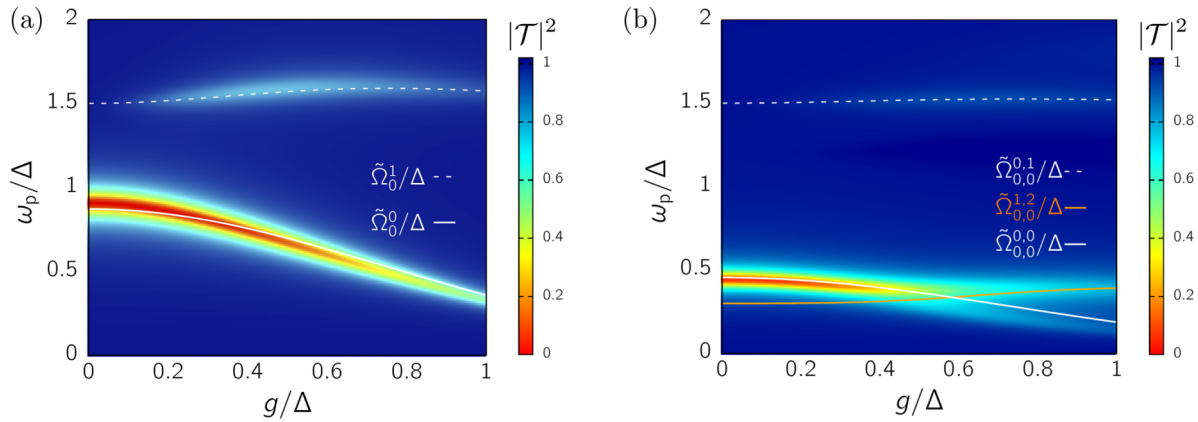


FIG. 5. Laguerre renormalization at $\epsilon_0 = 0$. Transmission at zero bias vs the qubit-resonator coupling g . (a) Static case, $\epsilon_d = 0$. (b) Driven case with $\epsilon_d = 4\Delta$. For both panels the other parameters are as in Fig. 4(b). Panel (a) displays, in the transition $\tilde{\Omega}_0^0$, the Laguerre pattern from L_0 . In panel (b), the splitting of the resonance is given by higher order Laguerre polynomials stemming from the interplay of the resonator with the drive [34]. The frequencies $\tilde{\Omega}_{n,j}^{m,l}$ are given by Eq. (14) with the substitution $\Delta \rightarrow \Delta_T$.

While transmission spectra generically carry information about spectral properties of the underlying quantum system being probed, the intensity and even the presence of resonance features crucially depend on which part of the system is coupled to the probe signal. Recent experiments by Yoshihara *et al.* [13] have provided spectroscopic data of the (undriven) Rabi model in the deep USC regime, with the probe on the resonator. In the setup considered in this work, the probe couples to the qubit. Hence, the relevant observed quantity is the population difference between the qubit's supercurrent states. This in turn implies, especially at strong dissipation, a different spectral response than so far reported in the literature [13,14]. To highlight the differences between the two probe settings, a comparison is provided in Appendix E; see also the experimental spectra in Figs. 2 and 3 of Ref. [13].

When probing the qubit, the strong coupling to the quantized resonator leads to sidebands in the spectrum, reflecting multiple absorption or emission of resonator's quanta. Furthermore, the doublet structure of the Rabi system is reflected in avoided crossings between subbands. When the drive is present, additional photon sidebands appear which also display avoided crossings. An advantage of this setup is the possibility of tuning the light-matter coupling in a continuous way. Indeed, the size and position of the avoided crossings depend on both the driving parameters as well as on the qubit-resonator coupling strength. Characteristic Bessel and Laguerre evolutions upon varying the driving and coupling strength witness the interplay between the classical drive and the resonator in the nonequilibrium steady-state response of the qubit.

The platform studied in this work is also suited for investigating the phenomenon of photon blockade [76,77], where a coherent drive on a cavity coupled to an artificial atom, the resonator-qubit system in our case, produces an output of single photons. Such a nonclassical resonator output can be detected by measuring the photon-photon correlation function $g^{(2)}(t)$ [78,79]. This phenomenon has been investigated in standard cavity-QED models described by the Jaynes-Cummings Hamiltonian [80,81] and the effects of the ultrastrong qubit-resonator coupling have been studied in

[79,82]. Since the phenomenon is ultimately due to the non-linearity of the artificial atom, it is reasonable to expect that a similar emission would be observed by coherently driving (and probing) the qubit. In support of this expectation, the experiment carried out in [83] already demonstrated photon blockade by a single qubit. Although the method used here is not suited for capturing the correlation function of the qubit output, an extension of the formalism in this direction could allow for studying how the phenomenon of photon blockade in a dissipative Rabi system is affected by driving and probing the qubit.

In summary, we presented theoretical predictions for the spectroscopy of the driven, dissipative Rabi model. Our results provide insight and tools to investigate the physics of USC systems. Furthermore, they can be used to optimize the design of future experiments and for the interpretation of spectroscopic results.

ACKNOWLEDGMENTS

The authors thank G. Falci and A. Ridolfo for fruitful discussions on the spectroscopy of the Rabi model. L.M. and M.G. acknowledge support by the BMBF (German Ministry for Education and Research), Project No. 13N15208, QuantERA SiUCs. P.F.-D. acknowledges support from a “la Caixa” Foundation junior leader fellowship (ID100010434-LCF/BQ/PR19/11700009), the Ministry of Science and Innovation and Agencia Estatal de Investigación (FIS2017-89860-P; SEV-2016-0588; PCI2019-111838-2), the European Commission (FET-Open AVaQus GA 899561; QuantERA SiUCs), and the program “Doctorat Industrial” of the Agency for Management of University and Research Grants (2020 DI 41; 2020 DI 42). IFAE is partially funded by the CERCA program of the Generalitat de Catalunya.

APPENDIX A: CALDEIRA-LEGGETT HAMILTONIAN AND SPECTRAL DENSITY FUNCTION

The Caldeira-Leggett model [60,61] describes an open system bilinearly interacting via the operator \hat{X} with a heat bath

of harmonic oscillators

$$H_{\text{CL}} = \frac{\hat{p}^2}{2M} + V(\hat{X}) + \frac{1}{2} \sum_{j=1}^N \left[\frac{\hat{p}_j^2}{m_j} + m_j \omega_j^2 \left(\hat{x}_j - \frac{c_j}{m_j \omega_j^2} \hat{X} \right)^2 \right]. \quad (\text{A1})$$

The interaction term is $\hat{X} \sum_j c_j \hat{x}_j$ and the spectral density function $J(\omega)$ is defined as

$$J(\omega) = \frac{\pi}{2} \sum_{j=1}^N \frac{c_j^2}{m_j \omega_j} \delta(\omega - \omega_j). \quad (\text{A2})$$

For a bosonic bath we have $\hat{x}_j = \sqrt{\hbar/2m_j\omega_j}(a_j + a_j^\dagger)$. Introducing the dimensionless system position operator $\hat{Q} := \hat{X}/X_0$ we can write

$$H_{\text{CL}} = H_S + \sum_l \hbar \omega_j a_j^\dagger a_j - \hat{Q} \sum_j \hbar \lambda_j (a_j + a_j^\dagger) + A^2, \quad (\text{A3})$$

where A^2 is proportional to the square of \hat{X} . If the open system is a qubit, this term is a constant since $\sigma_z^2 = \mathbf{1}$ while for a harmonic oscillator it constitutes a nonlinear term which ensures position-independent friction [21]. In Eq. (A3), we introduced the coupling with dimension of an angular frequency

$$\lambda_j = \frac{X_0}{\sqrt{2\hbar m_j \omega_j}} c_j.$$

In the context of the spin-boson model, it is also customary to define the modified spectral density function

$$G(\omega) := \sum_{j=1}^N \lambda_j^2 \delta(\omega - \omega_j) = \frac{X_0^2}{\pi \hbar} J(\omega). \quad (\text{A4})$$

For an Ohmic bath, in the continuum limit, $J(\omega) = M\gamma\omega$, where the friction coefficient γ coincides with the memoryless friction kernel in the corresponding generalized Langevin equation for the operator \hat{X} .

(i) If the system coupled to the bath is a harmonic oscillator then $\hat{X} = X_0(B^\dagger + B)$, with $X_0 = \sqrt{\hbar/2M\Omega}$. Setting $G(\omega) = \kappa\omega$, Eq. (A4) yields $\kappa = M\gamma X_0^2/(\pi/\hbar)$ and we can identify $\gamma = 2\pi\kappa\Omega$.

(ii) For a qubit coupled to the Ohmic bath the coupling coordinate is $\hat{X} = (X_0/2)\sigma_z$, where X_0 is the interwell distance [21]. The spin-boson spectral density function is defined as $G(\omega) = 2\alpha\omega$. From Eq. (A4) we have $\alpha = M\gamma X_0^2/(2\pi/\hbar)$.

APPENDIX B: THE DRIVEN, DISSIPATIVE RABI MODEL WITHIN NIBA

As shown in Sec. IV, the transmission is related to the response of the qubit to the probe field via the population difference $P(t) = \langle \sigma_z(t) \rangle$, i.e., the expectation value of σ_z , expressed in the localized (flux) states of the qubit. An exact formal expression for $P(t)$ in the presence of external heat baths, the Ohmic bath and the dissipative resonator in our case, and of a classical time-dependent drive is found within the path-integral representation of the qubit reduced dynamics [84,85].

The time evolution of the population difference can be given in terms of an exact generalized master equation (GME)

which reads [21,37]

$$\dot{P}(t) = \int_{t_0}^t dt' [K^-(t, t') - K^+(t, t')P(t')]. \quad (\text{B1})$$

In the presence of the time-dependent bias in Eq. (2), a closed form for the kernels of the GME (B1) is obtained within the noninteracting blip approximation (NIBA) [20,70]. The NIBA kernels are nonperturbative in the dissipation strength and the drive and read [37]

$$\begin{aligned} K^+(t, t') &= h^+(t - t') \cos[\zeta_{\text{full}}(t, t')], \\ K^-(t, t') &= h^-(t - t') \sin[\zeta_{\text{full}}(t, t')], \end{aligned} \quad (\text{B2})$$

with the dynamical phase reading

$$\begin{aligned} \zeta_{\text{full}}(t, t') &= \int_{t'}^t dt'' \epsilon(t'') \\ &= \epsilon_0(t - t') + \frac{\epsilon_p}{\omega_p} [\sin(\omega_p t) - \sin(\omega_p t')] \\ &\quad + \frac{\epsilon_d}{\omega_d} [\sin(\omega_d t) - \sin(\omega_d t')], \end{aligned} \quad (\text{B3})$$

and where

$$\begin{aligned} h^+(t) &= \Delta^2 e^{-Q'(t)} \cos[Q''(t)], \\ h^-(t) &= \Delta^2 e^{-Q'(t)} \sin[Q''(t)]. \end{aligned} \quad (\text{B4})$$

The baths' correlation function $Q(t)$ is the sum of the contributions from the different baths, $Q(t) = \sum_\nu Q_\nu(t)$ [72]. In our model, $Q(t) = Q_1(t) + Q_2(t)$, where the contribution from the Ohmic bath with exponential cutoff, acting directly on the qubit ($\nu = 1$), is, in the so-called scaling limit [21],

$$Q'_1(t) = 2\alpha_1 \ln \left[\sqrt{1 + \omega_c^2 t^2} \frac{\sinh[\pi t/(\hbar\beta_1)]}{\pi t/(\hbar\beta_1)} \right], \quad (\text{B5})$$

$$Q''_1(t) = 2\alpha_1 \arctan(\omega_c t). \quad (\text{B6})$$

Applying Eq. (23) to the spectral density function $G_2(\omega)$, Eq. (5), one obtains for the effective bath of the dissipative resonator ($\nu = 2$) [56,57,65]

$$\begin{aligned} Q'_2(t) &= Xt + L(e^{-\gamma t/2} \cos \bar{\Omega} t - 1) \\ &\quad - Ze^{-\gamma t/2} \sin \bar{\Omega} t + Q'_{\text{Mats}}(t), \end{aligned} \quad (\text{B7})$$

$$Q''_2(t) = \pi\alpha_2 - e^{-\gamma t/2} \pi\alpha_2 (\cos \bar{\Omega} t + N \sin \bar{\Omega} t), \quad (\text{B8})$$

with $X = 2\pi\alpha_2 k_B T/\hbar$ and $\bar{\Omega} = \sqrt{\Omega^2 - \gamma^2/4}$ and where

$$\begin{aligned} N &= \frac{\gamma^2/2 - \Omega^2}{\gamma \bar{\Omega}}, \\ L &= \pi\alpha_2 \frac{N \sinh(\beta \hbar \bar{\Omega}) + \sin(\beta \hbar \gamma/2)}{\cosh(\beta \hbar \bar{\Omega}) - \cos(\beta \hbar \gamma/2)}, \\ Z &= \pi\alpha_2 \frac{\sinh(\beta \hbar \bar{\Omega}) - N \sin(\beta \hbar \gamma/2)}{\cosh(\beta \hbar \bar{\Omega}) - \cos(\beta \hbar \gamma/2)}. \end{aligned} \quad (\text{B9})$$

The term $Q'_{\text{Mats}}(t)$ is the following series over the Matsubara frequencies $\nu_n := n 2\pi k_B T/\hbar$:

$$Q'_{\text{Mats}}(t) = 4\pi\alpha_2 \frac{\Omega^4}{\hbar\beta} \sum_{n=1}^{+\infty} \frac{1}{(\Omega^2 + \nu_n^2)^2 - \gamma^2 \nu_n^2} \left[\frac{1 - e^{-\nu_n t}}{\nu_n} \right]. \quad (\text{B10})$$

APPENDIX C: LINEAR SUSCEPTIBILITY IN THE PRESENCE OF A HIGH-FREQUENCY DRIVE

Averaging the kernels in Eq. (B2) over a drive period $T_d = 2\pi/\omega_d$, we make the substitution $K^\pm(t, t') \rightarrow K_d^\pm(t, t')$ in the GME, where

$$\begin{aligned} K_d^+(t, t') &= h_d^+(t - t') \cos[\zeta(t, t')], \\ K_d^-(t, t') &= h_d^-(t - t') \sin[\zeta(t, t')], \end{aligned} \quad (\text{C1})$$

with the dynamical phase $\zeta(t, t')$ which is now independent of the drive, as it contains exclusively the static bias and the time-dependent probe

$$\zeta(t, t') = \epsilon_0(t - t') + \frac{\epsilon_p}{\omega_p} [\sin(\omega_p t) - \sin(\omega_p t')]; \quad (\text{C2})$$

cf. Eq. (B3). The drive is taken into account effectively by the functions

$$\begin{aligned} h_d^+(t) &= \Delta^2 e^{-\mathcal{Q}^-(t)} \cos[\mathcal{Q}''(t)] J_0 \left[\frac{2\epsilon_d}{\omega_d} \sin\left(\frac{\omega_d t}{2}\right) \right], \\ h_d^-(t) &= \Delta^2 e^{-\mathcal{Q}^-(t)} \sin[\mathcal{Q}''(t)] J_0 \left[\frac{2\epsilon_d}{\omega_d} \sin\left(\frac{\omega_d t}{2}\right) \right]. \end{aligned} \quad (\text{C3})$$

The Bessel function can be expanded in Fourier series as

$$J_0 \left[\frac{2\epsilon_d}{\omega_d} \sin\left(\frac{\omega_d t}{2}\right) \right] = \sum_n J_n^2(\epsilon_d/\omega_d) e^{-in\omega_d t}. \quad (\text{C4})$$

Due to the effect of the monochromatic probe, we assume the asymptotic population difference $P_{\text{as}}(t)$ to be periodic with the period of the probe. The function $P_{\text{as}}(t)$ is the solution of the GME for $t_0 \rightarrow -\infty$, namely

$$\begin{aligned} \dot{P}_{\text{as}}(t) &= \int_{-\infty}^t dt' [K_d^-(t, t') - K_d^+(t, t') P_{\text{as}}(t')] \\ &= \int_0^\infty d\tau [K_d^-(t, t - \tau) - K_d^+(t, t - \tau) P_{\text{as}}(t - \tau)]. \end{aligned} \quad (\text{C5})$$

The NIBA kernels are periodical in t with the periodicity of the probe, and can be expanded in Fourier series as

$$K_d^\pm(t, t - \tau) = \sum_m k_m^\pm(\tau) e^{-i\omega_p t}, \quad (\text{C6})$$

where

$$k_m^\pm(\tau) = \frac{\omega_p}{2\pi} \int_{-\pi/\omega_p}^{\pi/\omega_p} dt K_d^\pm(t, t - \tau) e^{im\omega_p t}. \quad (\text{C7})$$

Defining $c^+(x) = \cos(x)$ and $c^-(x) = \sin(x)$, from Appendix D, we can write for $m = 0, 1$

$$\begin{aligned} k_0^\pm(\tau) &= h_d^\pm(\tau) c^\pm(\epsilon_0 \tau), \\ k_1^\pm(\tau) &= \mp \frac{\epsilon_p}{\omega_p} e^{i\omega_p \tau/2} h_d^\pm(\tau) \sin(\omega_p \tau/2) c^\mp(\epsilon_0 \tau), \end{aligned} \quad (\text{C8})$$

which are of order 0 and 1, respectively, in the ratio ϵ_p/ω_p .

Under the assumption that the memory time of the kernels is finite, $t_{\text{memory}} < \infty$, so that when the kernels are different from zero the asymptotic population different is already at the

steady state, $P(t) = P_{\text{as}}(t)$, we Fourier-expand $P_{\text{as}}(t)$ on the left-hand side and inside the integral in the GME (C5). The latter adopts the form

$$\begin{aligned} &\sum_m -im\omega_p p_m e^{-im\omega_p t} \\ &= \int_0^\infty d\tau \sum_m k_m^-(\tau) e^{-im\omega_p t} \\ &\quad - \int_0^\infty d\tau \sum_{m,n} k_m^+(\tau) e^{-i(m+n)\omega_p t} p_n e^{in\omega_p \tau}. \end{aligned}$$

Defining

$$\hat{k}_m^\pm(\lambda) = \int_0^\infty d\tau e^{-\lambda\tau} k_m^\pm(\tau), \quad (\text{C9})$$

Eq. (C9) reads

$$\begin{aligned} &\sum_m -im\omega_p p_m e^{-im\omega_p t} \\ &= \sum_m \hat{k}_m^-(0) e^{-im\omega_p t} - \sum_{m,n} \hat{k}_m^+(-in\omega_p) p_n e^{-i(m+n)\omega_p t}. \end{aligned} \quad (\text{C10})$$

Taking the component at frequency ω_p ,

$$-i\omega_p p_1 = \hat{k}_{+1}^-(0) - \sum_{m+n=1} \hat{k}_m^+(-in\omega_p) p_n. \quad (\text{C11})$$

Since $\hat{k}_m(\lambda) \propto (\epsilon_p/\omega_p)^{|m|}$, see Eq. (C8), we have

$$\begin{aligned} p_1(\omega_{\text{xp}}) &= \frac{1}{-i\omega_p + \hat{k}_0^+(-i\omega_p)} [\hat{k}_{+1}^-(0) - \hat{k}_{+1}^+(0) p_0] \\ &\quad + O[(\epsilon_p/\omega_p)^2]. \end{aligned} \quad (\text{C12})$$

Taking the zero-frequency component of Eq. (C9),

$$0 = \hat{k}_0^-(0) - \hat{k}_0^+(0) p_0 + O(\epsilon_p/\omega_p).$$

Thus, to the lowest order in the probe amplitude [37,86],

$$p_1(\omega_p) = \frac{1}{-i\omega_p + \hat{k}_0^+(-i\omega_p)} \left[\hat{k}_{+1}^-(0) - \hat{k}_{+1}^+(0) \frac{\hat{k}_0^-(0)}{\hat{k}_0^+(0)} \right], \quad (\text{C13})$$

where, from Eqs. (C8) and (C9),

$$\begin{aligned} \hat{k}_0^\pm(\lambda) &= \int_0^\infty d\tau e^{-\lambda\tau} h_d^\pm(\tau) c^\pm(\epsilon_0 \tau), \\ \hat{k}_1^\pm(0) &= \mp \frac{\epsilon_p}{\omega_p} \int_0^\infty d\tau e^{i\omega_p \tau/2} h_d^\pm(\tau) \sin(\omega_p \tau/2) c^\mp(\epsilon_0 \tau). \end{aligned} \quad (\text{C14})$$

The corresponding expression for the linear susceptibility $\chi(\omega_p) = p_1(\omega_p)/\hbar\epsilon_p$ is given in Eq. (21). This expression is the one used throughout the present work.

Markovian limit

For completeness we also give the susceptibility in the Markovian limit, namely when the decay time of the kernels is much shorter than the relevant timescales of variation of $P(t)$. In this case,

$$\dot{P}_{\text{as}}(t) = \int_0^\infty d\tau K_d^-(t, -\tau) - \int_0^\infty d\tau K_d^+(t, t - \tau) P_{\text{as}}(t). \quad (\text{C15})$$

By expanding the kernels in Fourier series we obtain the equation

$$\begin{aligned} & \sum_m -im\omega_p p_m e^{-im\omega_p t} \\ &= \sum_m \hat{k}_m^-(0) e^{-im\omega_p t} - \sum_{m,n} \hat{k}_m^+(0) p_n e^{-i(m+n)\omega_p t}, \end{aligned} \quad (\text{C16})$$

whose component at frequency ω_p is now

$$\begin{aligned} -i\omega_p p_1 &= \hat{k}_{+1}^-(0) - \sum_{m+n=1} \hat{k}_m^+(0) p_n e^{-i(m+n)\omega_p t} \\ &\simeq \hat{k}_{+1}^-(0) - \hat{k}_{+1}^+(0) p_0 - \hat{k}_0^+(0) p_{+1} - \hat{k}_{+2}^+(0) p_{-1}. \end{aligned} \quad (\text{C17})$$

As a result, in the Markovian limit and to the lowest order in ϵ_p/ω_p , we have

$$p_1(\omega_p) = \frac{1}{-i\omega_p + \hat{k}_0^+(0)} \left[\hat{k}_{+1}^-(0) - \hat{k}_{+1}^+(0) \frac{\hat{k}_0^-(0)}{\hat{k}_0^+(0)} \right]. \quad (\text{C18})$$

APPENDIX D: CALCULATION OF $k_m^\pm(\tau)$

We express the dynamical phase in Eq. (C2) as

$$\begin{aligned} \zeta(t, t - \tau) &= \epsilon_0 \tau + \frac{\epsilon_p}{\omega_p} \{ \sin(\omega_p t) - \sin[\omega_p(t - \tau)] \} \\ &= \epsilon_0 \tau + 2 \frac{\epsilon_p}{\omega_p} \cos(\omega_p t - \phi_\tau) \sin(\phi_\tau) \\ &= \epsilon_0 \tau + E(t, \tau), \end{aligned} \quad (\text{D1})$$

where $\phi_\tau := \omega_p \tau / 2$. Using the notation $c^+(x) := \cos(x)$ and $c^-(x) := \sin(x)$, the functions of the dynamical phase in Eq. (C1) read

$$c^\pm[\zeta(t, t - \tau)] = c^\pm(\epsilon_0 \tau) c^+[E(t, \tau)] \mp c^\mp(\epsilon_0 \tau) c^-[E(t, \tau)]. \quad (\text{D2})$$

As a result,

$$\begin{aligned} k_m^\pm(\tau) &= \frac{\omega_p}{2\pi} \int_{-\pi/\omega_p}^{\pi/\omega_p} dt K_d^\pm(t, t - \tau) e^{im\omega_p t} \\ &= h_d^\pm(\tau) \frac{\omega_p}{2\pi} \int_{-\pi/\omega_p}^{\pi/\omega_p} dt c^\pm[\zeta(t, t - \tau)] e^{im\omega_p t} \\ &= h_d^\pm(\tau) [c^\pm(\epsilon_0 \tau) F_m^+(\tau) \mp c^\mp(\epsilon_0 \tau) F_m^-(\tau)], \end{aligned} \quad (\text{D3})$$

where

$$\begin{aligned} F_m^\pm(\tau) &= \frac{\omega_p}{2\pi} \int_{-\pi/\omega_p}^{\pi/\omega_p} dt e^{im\omega_p t} c^\pm[E(t, \tau)] \\ &= \frac{e^{im\phi_\tau}}{2\pi} \int_{-\pi-\phi_\tau}^{\pi-\phi_\tau} dx c^\pm \left[\frac{2\epsilon_p}{\omega_p} \cos(x) \sin(\phi_\tau) \right] e^{imx} \\ &= \frac{e^{im\phi_\tau}}{2\pi} \int_{-\pi}^{\pi} dx c^\pm [z \cos(x)] e^{imx}, \end{aligned} \quad (\text{D4})$$

with $x := \omega_p t - \phi_\tau$ and $z := 2\epsilon_p \sin(\phi_\tau)/\omega_p$. In the last line we have shifted the integration domain (of length one period) exploiting the periodicity of the integrand. Since only the even part of the integrand contributes to the integral in Eq. (D4), we can write the latter as [71]

$$\begin{aligned} F_m^\pm(\tau) &= \frac{e^{im\phi_\tau}}{\pi} \int_0^\pi dx c^\pm [z \cos(x)] i^{(1\mp 1)/2} c^\pm(mx) \\ &= \frac{e^{im\phi_\tau}}{2\pi} \int_0^\pi dx [e^{iz \cos(x)} \pm e^{-iz \cos(x)}] c^\pm(mx) \\ &= e^{im\phi_\tau} i^{m-(1\mp 1)/2} \frac{J_m(z) \pm J_m(-z)}{2}, \end{aligned} \quad (\text{D5})$$

where J_m is the Bessel function of order m which has the parity $J_m(-z) = (-1)^m J_m(z)$. As a result

$$F_m^+(\tau) = \begin{cases} i^m e^{im\omega_p \tau/2} J_m \left[\frac{2\epsilon_p}{\omega_p} \sin \left(\frac{\omega_p \tau}{2} \right) \right], & m \text{ even,} \\ 0, & m \text{ odd,} \end{cases} \quad (\text{D6})$$

and

$$F_m^-(\tau) = \begin{cases} 0, & m \text{ even,} \\ \mp i^{m-1} e^{im\omega_p \tau/2} J_m \left[\frac{2\epsilon_p}{\omega_p} \sin \left(\frac{\omega_p \tau}{2} \right) \right], & m \text{ odd.} \end{cases} \quad (\text{D7})$$

To lowest order in z we have $J_m(z) \simeq (z/2)^m$. Then, substituting the above expressions for $F_m^\pm(\tau)$ into Eq. (D3), we obtain

$$\begin{aligned} k_m^\pm(\tau) &\simeq h_d^\pm(\tau) \\ &\times \begin{cases} i^m e^{im\omega_p \tau/2} \left[\frac{\epsilon_p}{\omega_p} \sin \left(\frac{\omega_p \tau}{2} \right) \right]^m c^\pm(\epsilon_0 \tau), & m \text{ even,} \\ \mp i^{m-1} e^{im\omega_p \tau/2} \left[\frac{\epsilon_p}{\omega_p} \sin \left(\frac{\omega_p \tau}{2} \right) \right]^m c^\mp(\epsilon_0 \tau), & m \text{ odd,} \end{cases} \end{aligned} \quad (\text{D8})$$

to lowest order in ϵ_p/ω_p .

APPENDIX E: COMPARISON WITH THE PROBE ON THE RESONATOR

In contrast to the situation addressed in the present work, where the qubit is probed, standard spectroscopy on USC systems [13] is performed by probing the resonator, namely the operator \hat{X} that couples to the transmission line is proportional to resonator position operator, $\hat{X} \propto B^\dagger + B$. In order to highlight the differences in the spectra, in Fig. 6 we compare the transmission for the two probe settings in the weak-dissipation regime. As done in Fig. 2(a), the qubit susceptibility is calculated according to the approach in [58] with dephasing rates from the Bloch-Redfield master equation in the dressed basis of the USC system. The spectra are shown for the same set of values of the qubit-resonator coupling as in Fig. 2, but this time at resonance, $\Omega = \Delta$. In both probe settings, the spectra

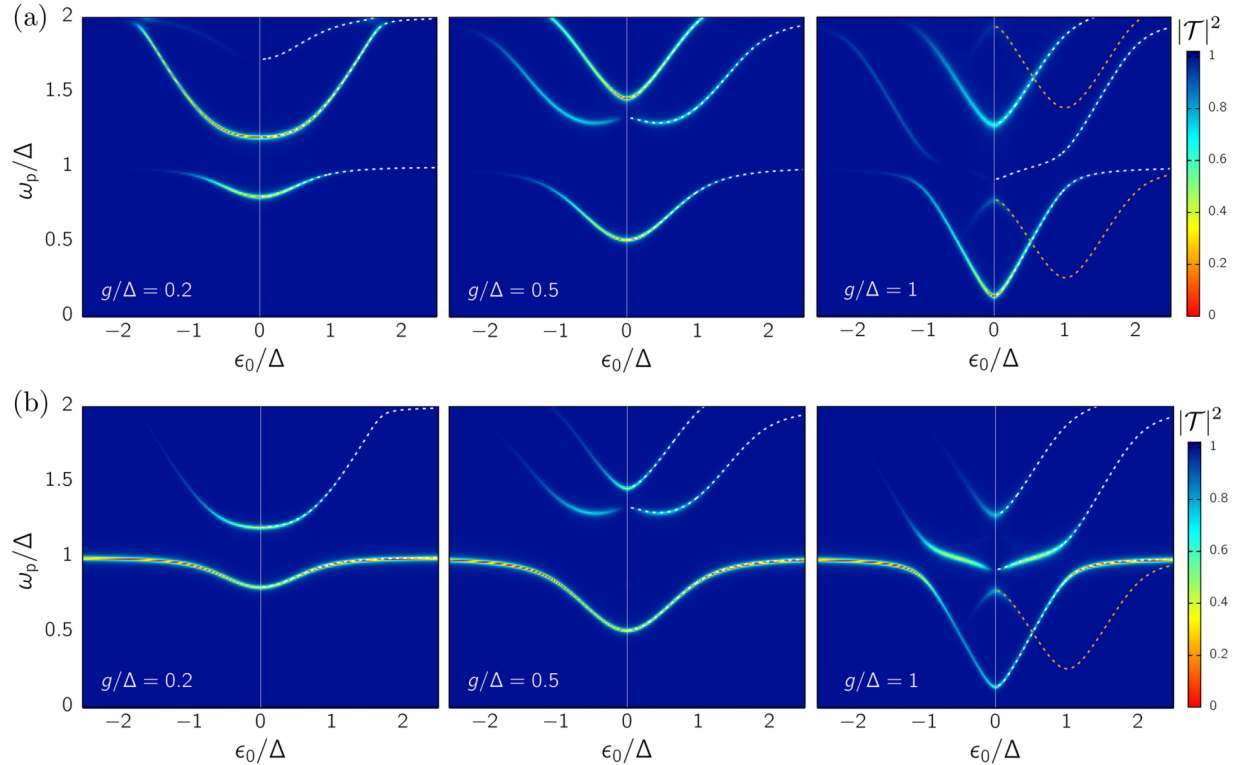


FIG. 6. Transmission spectra of the static system in the weak-dissipation regime ($\alpha_1 = \kappa = 0.005$) at resonance, $\Omega = \Delta$, for different values of the qubit-resonator coupling g . (a) Probe on the qubit. (b) Probe on the resonator. For both panels, the transmission is evaluated using Eq. (20) and the susceptibility is calculated using the approach of [58] with dephasing rates within a Bloch-Redfield master equation approach. The white (orange) dashed lines mark the numerically evaluated transition energies between the ground (first excited) and the higher excited states. The remaining parameters are the same as in Fig. 2(a).

display resonances corresponding to the transition energies of the Rabi model, with a linewidth given by the decoherence rates, and no environment-induced renormalization of the resonances' positions, which is neglected by the theory and assumed to be small. The results for the probe on the qubit, Fig. 6(a), display complementary features with respect to the ones obtained with the probe on the resonator, Fig. 6(b). In the first setting, similarly to Fig. 2, resonances are suppressed outside the region $\omega_p > |\epsilon_0|$. On the contrary, when the probe is on the resonator the horizontal features, which are insensitive to changes in the static bias, are the most pronounced. We also note that the qubit spectrum with the largest qubit-resonator coupling, $g = \Delta$ in Fig. 6(a), resembles the ones at strong dissipation in Fig. 2(b). The reason is the strong renormalization effect on the bare qubit splitting Δ , in this case exerted by the resonator at resonance, which depends on the ratio g/Ω ; see Eq. (11).

APPENDIX F: INTERMEDIATE-DISSIPATION REGIME

In Fig. 7, we compare the results from the weak-dissipation approach used in Figs. 2(a) and 6 with the ones from the path-integral approach within NIBA. In both panels (a) and (b) of Fig. 7 we show, for reference, the numerically evaluated transition energies of the closed Rabi model. Based on

the validity of the NIBA at zero static bias we can make two observations. First, both approaches reproduce the main resonance involving the ground/first excited state, as given by the numerical diagonalization of the closed Rabi Hamiltonian, meaning that the bath-induced renormalization of the qubit frequency is not an important effect in the intermediate regime considered here, $\alpha = 0.01$ and $\kappa = 0.05$. Second, the weak-coupling approach fails to capture the renormalization of the resonances involving excited states higher than the first; see panel (b) of Fig. 7. On the other hand, one would expect to still be able to observe, even if reduced to some degree, the avoided crossings present in Fig. 7(a) which are completely suppressed in the NIBA results of panel (b).

In the intermediate-dissipation regime considered here, signatures of the bath-induced renormalization of the system's bare frequencies and the transition to the strong-dissipation regime analyzed in Sec. V are expected to be revealed in the spectra. We note however, that in this intermediate regime the use of accurate numerical treatments to check the validity of both approximation schemes might be appropriate. These are, for example, the quasiadiabatic path-integral approach [52] applied to the spin-boson model with the effective bath mapping used here for the NIBA, or the matrix-product state ansatz based on a chain mapping of the full Hamiltonian [66].

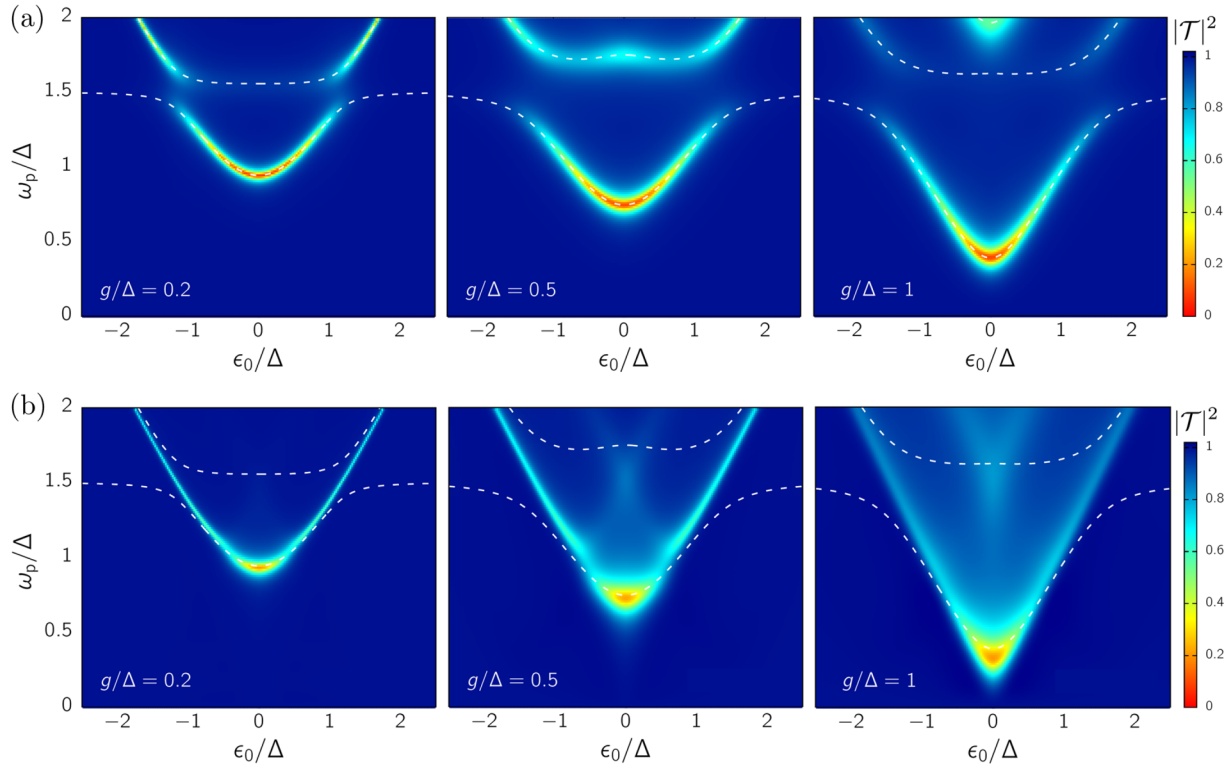


FIG. 7. Transmission spectra of the static system with probe on the qubit in the intermediate-dissipation regime, $\alpha_1 = 0.01$ and $\kappa = 0.05$, for different values of the qubit-resonator coupling g . For both panels, the transmission is evaluated using Eq. (20) and the susceptibility is calculated using (a) the approach of [58] with dephasing rates within a Bloch-Redfield master equation approach and (b) the path-integral approach within NIBA. In both panels, the white dashed lines show, for reference, the numerically evaluated transition energies between the ground and higher excited states of the closed Rabi model. The remaining parameters are the same as in Fig. 2.

-
- [1] J. Q. You and F. Nori, Atomic physics and quantum optics using superconducting circuits, *Nature (London)* **474**, 589 (2011).
- [2] A. A. Houck, H. E. Türeci, and J. Koch, On-chip quantum simulation with superconducting circuits, *Nat. Phys.* **8**, 292 (2012).
- [3] J. P. Pekola, Towards quantum thermodynamics in electronic circuits, *Nat. Phys.* **11**, 118 (2015).
- [4] G. Wendin, Quantum information processing with superconducting circuits: A review, *Rep. Prog. Phys.* **80**, 106001 (2017).
- [5] X. Gu, A. F. Kockum, A. Miranowicz, Y.-X. Liu, and F. Nori, Microwave photonics with superconducting quantum circuits, *Phys. Rep.* **718-719**, 1 (2017).
- [6] C. Ciuti, G. Bastard, and I. Carusotto, Quantum vacuum properties of the intersubband cavity polariton field, *Phys. Rev. B* **72**, 115303 (2005).
- [7] J. Bourassa, J. M. Gambetta, A. A. Abdumalikov, O. Astafiev, Y. Nakamura, and A. Blais, Ultrastrong coupling regime of cavity QED with phase-biased flux qubits, *Phys. Rev. A* **80**, 032109 (2009).
- [8] J. Hausinger and M. Grifoni, Dissipative dynamics of a biased qubit coupled to a harmonic oscillator: Analytical results beyond the rotating wave approximation, *New J. Phys.* **10**, 115015 (2008).
- [9] T. Niemczyk *et al.*, Circuit quantum electrodynamics in the ultrastrong-coupling regime, *Nat. Phys.* **6**, 772 (2010).
- [10] S. Ashhab and F. Nori, Qubit-oscillator systems in the ultrastrong-coupling regime and their potential for preparing nonclassical states, *Phys. Rev. A* **81**, 042311 (2010).
- [11] J. Hausinger and M. Grifoni, Qubit-oscillator system: An analytical treatment of the ultrastrong coupling regime, *Phys. Rev. A* **82**, 062320 (2010).
- [12] P. Forn-Díaz, J. Lisenfeld, D. Marcos, J. J. García-Ripoll, E. Solano, C. J. P. M. Harmans, and J. E. Mooij, Observation of the Bloch-Siegert Shift in a Qubit-Oscillator System in the Ultrastrong Coupling Regime, *Phys. Rev. Lett.* **105**, 237001 (2010).
- [13] F. Yoshihara, T. Fuse, S. Ashhab, K. Kakuyanagi, S. Saito, and K. Semba, Superconducting qubit-oscillator circuit beyond the ultrastrong-coupling regime, *Nat. Phys.* **13**, 44 (2017).
- [14] F. Yoshihara, T. Fuse, S. Ashhab, K. Kakuyanagi, S. Saito, and K. Semba, Characteristic spectra of circuit quantum electrodynamics systems from the ultrastrong- to the deep-strong-coupling regime, *Phys. Rev. A* **95**, 053824 (2017).
- [15] P. Forn-Díaz, L. Lamata, E. Rico, J. Kono, and E. Solano, Ultrastrong coupling regimes of light-matter interaction, *Rev. Mod. Phys.* **91**, 025005 (2019).

- [16] F. A. Kockum, A. Miranowicz, S. De Liberato, S. Savasta, and F. Nori, Ultrastrong coupling between light and matter, *Nat. Rev. Phys.* **1**, 19 (2019).
- [17] G. Romero, D. Ballester, Y. M. Wang, V. Scarani, and E. Solano, Ultrafast Quantum Gates in Circuit QED, *Phys. Rev. Lett.* **108**, 120501 (2012).
- [18] M.H. Devoret and J.M. Martinis, Implementing qubits with superconducting integrated circuits, *Quantum Inf. Process.* **3**, 163 (2004).
- [19] J. E. Mooij, T. P. Orlando, L. Levitov, L. Tian, C. H. van der Wal, and S. Lloyd, Josephson persistent-current qubit, *Science* **285**, 1036 (1999).
- [20] A. J. Leggett, S. Chakravarty, A. T. Dorsey, M. P. A. Fisher, A. Garg, and W. Zwerger, Dynamics of the dissipative two-state system, *Rev. Mod. Phys.* **59**, 1 (1987).
- [21] U. Weiss, *Quantum Dissipative Systems*, 4th ed. (World Scientific, Singapore, 2012).
- [22] H. P. Breuer and F. Petruccione, *The Theory of Open Quantum Systems* (Oxford University Press, Oxford, 2002).
- [23] B. Peropadre, D. Zueco, D. Porras, and J. J. García-Ripoll, Nonequilibrium and Nonperturbative Dynamics of Ultrastrong Coupling in Open Lines, *Phys. Rev. Lett.* **111**, 243602 (2013).
- [24] P. Forn-Díaz, J. J. García-Ripoll, B. Peropadre, J. L. Orgiazzi, M. A. Yurtalan, R. Belyansky, C. M. Wilson, and A. Lupascu, Ultrastrong coupling of a single artificial atom to an electromagnetic continuum in the nonperturbative regime, *Nat. Phys.* **13**, 39 (2017).
- [25] L. Magazzù, P. Forn-Díaz, R. Belyansky, J.-L. Orgiazzi, M. A. Yurtalan, M. R. Otto, A. Lupascu, C. M. Wilson, and M. Grifoni, Probing the strongly driven spin-boson model in a superconducting quantum circuit, *Nat. Commun.* **9**, 1403 (2018).
- [26] J. Leppäkangas, J. Braumüller, M. Hauck, J.-M. Reiner, I. Schwenk, S. Zanker, L. Fritz, A. V. Ustinov, M. Weides, and M. Marthaler, Quantum simulation of the spin-boson model with a microwave circuit, *Phys. Rev. A* **97**, 052321 (2018).
- [27] P. M. Javier, L. Sébastien, N. Gheeraert, R. Dassonneville, L. Planat, F. Foroughi, Y. Krupko, O. Buisson, C. Naud, W. Hasch-Guichard, S. Florens, I. Snyman, and N. Roch, A tunable Josephson platform to explore many-body quantum optics in circuit-QED, *npj Quantum Inf.* **5**, 19 (2019).
- [28] R. Kuzmin, N. Mehta, N. Grabon, R. Mencia, and V. E. Manucharyan, Superstrong coupling in circuit quantum electrodynamics, *npj Quantum Inf.* **5**, 20 (2019).
- [29] D. Z. Rossatto, C. J. Villas-Bôas, M. Sanz, and E. Solano, Spectral classification of coupling regimes in the quantum Rabi model, *Phys. Rev. A* **96**, 013849 (2017).
- [30] G. Díaz-Camacho, A. Bermudez, and J. J. García-Ripoll, Dynamical polaron ansatz: A theoretical tool for the ultrastrong-coupling regime of circuit QED, *Phys. Rev. A* **93**, 043843 (2016).
- [31] F. Armata, G. Calajo, T. Jaako, M. S. Kim, and P. Rabl, Harvesting Multiqubit Entanglement from Ultrastrong Interactions in Circuit Quantum Electrodynamics, *Phys. Rev. Lett.* **119**, 183602 (2017).
- [32] D. De Bernardis, P. Pilar, T. Jaako, S. De Liberato, and P. Rabl, Breakdown of gauge invariance in ultrastrong-coupling cavity QED, *Phys. Rev. A* **98**, 053819 (2018).
- [33] O. Di Stefano, A. Settineri, V. Macrì, L. Garziano, R. Stassi, S. Savasta, and F. Nori, Resolution of gauge ambiguities in ultrastrong-coupling cavity quantum electrodynamics, *Nat. Phys.* **15**, 803 (2019).
- [34] J. Hausinger and M. Grifoni, Qubit-oscillator system under ultrastrong coupling and extreme driving, *Phys. Rev. A* **83**, 030301(R) (2011).
- [35] W. D. Oliver, Y. Yu, J. C. Lee, K. K. Berggren, L. S. Levitov, and T. P. Orlando, Mach-Zehnder interferometry in a strongly driven superconducting qubit, *Science* **310**, 1653 (2005).
- [36] C. M. Wilson, T. Duty, F. Persson, M. Sandberg, G. Johansson, and P. Delsing, Coherence Times of Dressed States of a Superconducting Qubit under Extreme Driving, *Phys. Rev. Lett.* **98**, 257003 (2007).
- [37] M. Grifoni and P. Hänggi, Driven quantum tunneling, *Phys. Rep.* **304**, 229 (1998).
- [38] J. Hausinger and M. Grifoni, Dissipative two-level system under strong ac driving: A combination of Floquet and Van Vleck perturbation theory, *Phys. Rev. A* **81**, 022117 (2010).
- [39] S. Kohler, Dispersive Readout of Adiabatic Phases, *Phys. Rev. Lett.* **119**, 196802 (2017).
- [40] G. Engelhardt and J. Cao, Dynamical Symmetries and Symmetry-Protected Selection Rules in Periodically Driven Quantum Systems, *Phys. Rev. Lett.* **126**, 090601 (2021).
- [41] V. Reimer, K. G. L. Pedersen, N. Tanger, M. Pletyukhov, and V. Gritsev, Nonadiabatic effects in periodically driven dissipative open quantum systems, *Phys. Rev. A* **97**, 043851 (2018).
- [42] F. Yoshihara, T. Fuse, Z. Ao, S. Ashhab, K. Kakuyanagi, S. Saito, T. Aoki, K. Koshino, and K. Semba, Inversion of Qubit Energy Levels in Qubit-Oscillator Circuits in the Deep-Strong-Coupling Regime, *Phys. Rev. Lett.* **120**, 183601 (2018).
- [43] J. Lolli, A. Baksic, D. Nagy, V. E. Manucharyan, and C. Ciuti, Ancillary Qubit Spectroscopy of Vacua in Cavity and Circuit Quantum Electrodynamics, *Phys. Rev. Lett.* **114**, 183601 (2015).
- [44] G. Falci, A. Ridolfo, P. G. Di Stefano, and E. Paladino, Ultrastrong coupling probed by coherent population transfer, *Sci. Rep.* **9**, 9249 (2019).
- [45] A. Ridolfo, G. Falci, F. M. D. Pellegrino, G. D. Maccarrone, and E. Paladino, Photon pair production by STIRAP in ultrastrongly coupled matter-radiation systems, *Eur. Phys. J.: Spec. Top.* **227**, 2183 (2019).
- [46] O. Astafiev, A. M. Zagoskin, A. A. Abdumalikov, Y. A. Pashkin, T. Yamamoto, K. Inomata, Y. Nakamura, and J. S. Tsai, Resonance fluorescence of a single artificial atom, *Science* **327**, 840 (2010).
- [47] I.-C. Hoi, C. M. Wilson, G. Johansson, T. Palomaki, B. Peropadre, and P. Delsing, Demonstration of a Single-Photon Router in the Microwave Regime, *Phys. Rev. Lett.* **107**, 073601 (2011).
- [48] A. A. Abdumalikov, O. V. Astafiev, Y. A. Pashkin, Y. Nakamura, and J. S. Tsai, Dynamics of Coherent and Incoherent Emission from an Artificial Atom in a 1D Space, *Phys. Rev. Lett.* **107**, 043604 (2011).
- [49] M. Haerberlein *et al.*, Spin-boson model with an engineered reservoir in circuit quantum electrodynamics, [arXiv:1506.09114](https://arxiv.org/abs/1506.09114).
- [50] P. Forn-Díaz, C. W. Warren, C. W. S. Chang, A. M. Vadiraj, and C. M. Wilson, On-Demand Microwave Generator of Shaped Single Photons, *Phys. Rev. Appl.* **8**, 054015 (2017).
- [51] I. Chiorescu, P. Bertet, K. Semba, Y. Nakamura, C. J. P. M. Harmans, and J. E. Mooij, Coherent dynamics of a flux qubit

- coupled to a harmonic oscillator, *Nature (London)* **431**, 159 (2004).
- [52] M. Thorwart, E. Paladino, and M. Grifoni, Dynamics of the spin-boson model with a structured environment, *Chem. Phys* **296**, 333 (2004).
- [53] J. Johansson, S. Saito, T. Meno, H. Nakano, M. Ueda, K. Semba, and H. Takayanagi, Vacuum Rabi Oscillations in a Macroscopic Superconducting Qubit *LC* Oscillator System, *Phys. Rev. Lett.* **96**, 127006 (2006).
- [54] A. Ronzani, B. Karimi, J. Senior, Y.-C. Chang, J. T. Peltonen, C.D. Chen, and J. P. Pekola, Tunable photonic heat transport in a quantum heat valve, *Nat. Phys.* **14**, 991 (2018).
- [55] F. Beaudoin, J. M. Gambetta, and A. Blais, Dissipation and ultrastrong coupling in circuit QED, *Phys. Rev. A* **84**, 043832 (2011).
- [56] A. Garg, J. N. Onuchic, and V. Ambegaokar, Effect of friction on electron transfer in biomolecules, *J. Chem. Phys.* **83**, 4491 (1985).
- [57] L. Magazzù and M. Grifoni, Transmission spectra of an ultrastrongly coupled qubit-dissipative resonator system, *J. Stat. Mech.* (2019) 104002.
- [58] S. Kohler, Dispersive readout: Universal theory beyond the rotating-wave approximation, *Phys. Rev. A* **98**, 023849 (2018).
- [59] S. De Liberato, D. Gerace, I. Carusotto, and C. Ciuti, Extracavity quantum vacuum radiation from a single qubit, *Phys. Rev. A* **80**, 053810 (2009).
- [60] A. O. Caldeira and A. J. Leggett, Influence of Dissipation on Quantum Tunneling in Macroscopic Systems, *Phys. Rev. Lett.* **46**, 211 (1981).
- [61] A. O. Caldeira and A. J. Leggett, Quantum tunnelling in a dissipative system, *Ann. Phys.* **149**, 374 (1983).
- [62] N. Maleeva *et al.*, Circuit quantum electrodynamics of granular aluminum resonators, *Nat. Commun.* **9**, 3889 (2018).
- [63] L. Grünhaupt *et al.*, Granular aluminium as a superconducting material for high-impedance quantum circuits, *Nat. Mater.* **18**, 816 (2019).
- [64] M. C. Goorden, M. Thorwart, and M. Grifoni, Entanglement Spectroscopy of a Driven Solid-State Qubit and Its Detector, *Phys. Rev. Lett.* **93**, 267005 (2004).
- [65] F. Nesi, M. Grifoni, and E. Paladino, Dynamics of a qubit coupled to a broadened harmonic mode at finite detuning, *New J. Phys.* **9**, 316 (2007).
- [66] D. Zueco and J. J. García-Ripoll, Ultrastrongly dissipative quantum Rabi model, *Phys. Rev. A* **99**, 013807 (2019).
- [67] E. K. Irish, J. Gea-Banacloche, I. Martin, and K. C. Schwab, Dynamics of a two-level system strongly coupled to a high-frequency quantum oscillator, *Phys. Rev. B* **72**, 195410 (2005).
- [68] E. K. Irish, Generalized Rotating-Wave Approximation for Arbitrarily Large Coupling, *Phys. Rev. Lett.* **99**, 173601 (2007).
- [69] U. Vool and M. Devoret, Introduction to quantum electromagnetic circuits, *Int. J. Circuit Theory Appl.* **45**, 897 (2017).
- [70] H. Dekker, Noninteracting-blip approximation for a two-level system coupled to a heat bath, *Phys. Rev. A* **35**, 1436 (1987).
- [71] I. S. Gradshteyn and I. M. Ryzhik, *Table of Integrals, Series, and Products* (Academic Press, New York, 1980).
- [72] L. Nicolin and D. Segal, Non-equilibrium spin-boson model: Counting statistics and the heat exchange fluctuation theorem, *J. Chem. Phys.* **135**, 164106 (2011).
- [73] N. Boudjada and D. Segal, From dissipative dynamics to studies of heat transfer at the nanoscale: Analysis of the spin-boson model, *J. Phys. Chem. A* **118**, 11323 (2014).
- [74] D. Segal, Heat transfer in the spin-boson model: A comparative study in the incoherent tunneling regime, *Phys. Rev. E* **90**, 012148 (2014).
- [75] T. Yamamoto, M. Kato, T. Kato, and K. Saito, Heat transport via a local two-state system near thermal equilibrium, *New J. Phys.* **20**, 093014 (2018).
- [76] A. Imamoglu, H. Schmidt, G. Woods, and M. Deutsch, Strongly Interacting Photons in a Nonlinear Cavity, *Phys. Rev. Lett.* **79**, 1467 (1997).
- [77] K. M. Birnbaum, A. Boca, R. Miller, A. D. Boozer, T. E. Northup, and H. J. Kimble, Photon blockade in an optical cavity with one trapped atom, *Nature (London)* **436**, 87 (2005).
- [78] A. J. Hoffman, S. J. Srinivasan, S. Schmidt, L. Spietz, J. Aumentado, H. E. Türeci, and A. A. Houck, Dispersive Photon Blockade in a Superconducting Circuit, *Phys. Rev. Lett.* **107**, 053602 (2011).
- [79] A. Ridolfo, M. Leib, S. Savasta, and M. J. Hartmann, Photon Blockade in the Ultrastrong Coupling Regime, *Phys. Rev. Lett.* **109**, 193602 (2012).
- [80] H. J. Carmichael, Breakdown of Photon Blockade: A Dissipative Quantum Phase Transition in Zero Dimensions, *Phys. Rev. X* **5**, 031028 (2015).
- [81] J. B. Curtis, I. Boettcher, J. T. Young, M. F. Maghrebi, H. Carmichael, A. V. Gorshkov, and M. Foss-Feig, Critical theory for the breakdown of photon blockade, *Phys. Rev. Research* **3**, 023062 (2021).
- [82] A. Le Boité, M.-J. Hwang, H. Nha, and M. B. Plenio, Fate of photon blockade in the deep strong-coupling regime, *Phys. Rev. A* **94**, 033827 (2016).
- [83] I.-C. Hoi, T. Palomaki, J. Lindkvist, G. Johansson, P. Delsing, and C. M. Wilson, Generation of Nonclassical Microwave States Using an Artificial Atom in 1D Open Space, *Phys. Rev. Lett.* **108**, 263601 (2012).
- [84] M. Carrega, P. Solinas, A. Braggio, M. Sassetti, and U. Weiss, Functional integral approach to time-dependent heat exchange in open quantum systems: General method and applications, *New J. Phys.* **17**, 045030 (2015).
- [85] M. Carrega, P. Solinas, M. Sassetti, and U. Weiss, Energy Exchange in Driven Open Quantum Systems at Strong Coupling, *Phys. Rev. Lett.* **116**, 240403 (2016).
- [86] M. Grifoni, M. Sassetti, P. Hänggi, and U. Weiss, Cooperative effects in the nonlinearly driven spin-boson system, *Phys. Rev. E* **52**, 3596 (1995).